HAL
open science

SLX4 interacts with RTEL1 to prevent transcription-mediated DNA replication perturbations

A. Takedachi, E. Despras, S. Scaglione, R. Guérois, J. Guervilly, M. Blin, S. Audebert, L. Camoin, Z. Hasanova, M. Schertzer, et al.

To cite this version:

A. Takedachi, E. Despras, S. Scaglione, R. Guérois, J. Guervilly, et al.. SLX4 interacts with RTEL1 to prevent transcription-mediated DNA replication perturbations. Nature Structural and Molecular Biology, 2020, 27 (5), pp.438-449. 10.1038/s41594-020-0419-3 . hal-03079782

HAL Id: hal-03079782

https://hal.science/hal-03079782

Submitted on 17 Dec 2020

HAL is a multi-disciplinary open access archive for the deposit and dissemination of scientific research documents, whether they are published or not. The documents may come from teaching and research institutions in France or abroad, or from public or private research centers.

L'archive ouverte pluridisciplinaire **HAL**, est destinée au dépôt et à la diffusion de documents scientifiques de niveau recherche, publiés ou non, émanant des établissements d'enseignement et de recherche français ou étrangers, des laboratoires publics ou privés.

Figure #	Figure title One sentence only	Filename This should be the name the file is saved as when it is uploaded to our system. Please include the file extension. i.e.: *Smith_ED_Fig1.jpg*	Figure Legend If you are citing a reference for the first time in these legends, please include all new references in the Online Methods References section, and carry on the numbering from the main References section of the paper.
Extended Data Fig. 1	**RTEL1 is a binding partner of SLX4**	NSMB_A41514B_Takedachi_Extended_Data_Fig_1_final.jpg	**(**a) YFP-pull down from HeLa cells expressing YFP-SLX4. In lanes 3, 4 and 5 YFP-pull downs were washed in a high salt buffer (NaCl) or carried out in the presence of Benzonase (Benzo) or Ethidium bromide (EtBr) (See Methods). MUS81 and XPF were used as positive controls for SLX4-binding. (b) Endogenous SLX4 was immunoprecipitated from a HeLa cell-lysate with a combination of two different anti-SLX4 antibodies (See methods). (c) Immunoprecipitation of Flag-HA-SLX4 from dox-inducible HeLa cells at various time points after release from a thymidine block. Cell cycle profiles of the samples (left). Immunoblot of a representative experiment (right) and the quantifications of three independent experiments (mean with SEM). (d) RTEL1-binding domain of SLX4 and multiple SLX4 sequence alignment centred on the region 599-635 of human SLX4. Top two sequences report secondary structures (H: helix) and disorder status (D) predicted by PSIPRED and SPOTD algorithms, respectively (See Methods). NCBI RefSeq identifiers are given within brackets. UBZ4: ubiquitin-binding, MLR: primary XPF-binding domain, BTB: homodimerization domain (also contributes to XPF-binding), TBM: TRF2-binding motif, SIM: SUMO-interacting motifs, SAP: MUS81-binding region, CCD: SLX1-binding domain. (e) YFP-pull downs from HeLa cells expressing WT or mutated YFP-SLX4. ΔBTB: M_{684}VNN-GLPP$_{764}$ was deleted from the BTB domain. BTB5A and SIM: point mutations in the BTB domain and SIM motifs, respectively, as described in[2]. D614G and L618P: cancer-associated

			mutations (Fig. 1d). (f) YFP-pull downs from HeLa cells expressing WT or mutated YFP-SLX4. L1022A: TRF2-binding defective mutant. All immunoblots were performed with antibodies against the indicated proteins. Uncropped images for panels a,b,d,e,f and data for graphs in panel b are available as source data.
Extended Data Fig. 2	**List of known SLX4 interactors identified in YFP-SLX4 pull down**	NSMB_A41514B_Takedachi_Extended_Data_Fig_2_final_new.jpg	List of all known SLX4 interactors (light green) and RTEL1 (dark green) that were identified in the YFP-SLX4 pull down shown in Extended Data 1a. The table shows a spectral counting based on the number of peptide-to-spectrum matching (PSM) events. (see Supplementary Note for Mass spectrometry and data analysis methods and Supplementary Table 1 for the full data report).
Extended Data Fig. 3	**List of SLX4 partners impacted by the D614G and L618P SLX4 mutations**	NSMB_A41514B_Takedachi_Extended_Data_Fig_3_final_new.jpg	List of all proteins identified in all three runs of the wild-type YFP-SLX4$_{577-795}$ sample but in none of the runs of the D614G and L618P mutated samples or the HeLa "Fit0" (HeLa Flp-In TREX cells with no SLX4 cDNA integrated at the FRT site) negative control (see Supplementary Table 4 for the mass spectrometry data full report). The table shows a spectral counting based on the number of peptide-to-spectrum matching (PSM) events. (see Supplementary Note for Mass spectrometry and data analysis methods and Supplementary Table 1 for the data full report).
Extended Data Fig. 4	**SLX4 binds HD1 of RTEL1**	NSMB_A41514B_Takedachi_Extended_Data_Fig_4_final_new.jpg	(a) Multiple sequence alignment of RTEL1 homologs focused on the region 888-1156 of human RTEL1. Top two sequences report the secondary structures (H for helix) and disorder status (D) predicted by PSIPRED and SPOTD algorithms, respectively (See Methods). Blue boxes indicate the delimitation of the canonical harmonin/PAH domains HD1 and HD2 and the red box spots out the extension required for interaction with SLX4. For species having diverged before the emergence of bony fishes, the

			second harmonin domain is not present. NCBI RefSeq identifiers are given within brackets. (b) *E. coli* produced 6His-tagged HD1a ($RTEL1_{885-975}$), HD1b ($RTEL1_{885-990}$) and HD2a ($RTEL1_{1046-1142}$) fragments were used in a Ni++-pull down *in vitro* assay to monitor their interaction with a GST-tagged $SLX4_{577-1042}$ (Helix+BTB) fragment. The first and last lanes represent the inputs of the Ni++-pull down assays. B: Ni++-beads, Ft: Flow through. The pelleted beads were resuspended in a volume of Laemmli buffer equivalent to the initial volume of the binding assay. Identical volumes of the GST-tagged $SLX4_{577-1042}$ (Helix+BTB) fragment (diluted to the final concentration used in the binding assay), the B and the Ft samples were loaded on the gel. (c) Schematic representation of the RTEL1 fragment (Top) used in Y2H to assess direct binding to the $SLX4_{577-1042}$ fragment. K897E: Hoyeraal-Hreidarsson syndrome (HHS) associated mutation. Bottom panel shows Y2H to assess direct binding between the RTEL1 fragments and $SLX4_{577-1042}$ (Helix+BTB) fragment. (d) Schematic representation of the YFP-tagged RTEL1 fragments (Top) used in the YFP-pull down to assess binding to endogenous SLX4 (Bottom). All indicated RTEL1 point mutations are from Hoyeraal-Hreidarsson syndrome (HHS) patients[31]. Uncropped images of the immunoblots in panels b,d and Y2H in c are available as source data.
Extended Data Fig. 5	**Interaction between SLX4 and RTEL1 is required for proper replication fork progression but not for ICL repair**	NSMB_A41514B_Takedachi_Extended_Data_Fig_5_final_new.jpg	(a) Colony survival assay with mock-depleted (siLUC) and SLX4-depleted (siUTR) HeLa “Fit0” and HeLa Flp-In TREX cells expressing WT or mutated Flag-HA-SLX4 as indicated treated with MMC for 24 hrs. Values represent the means and SEM from three independent experiments. The Immunoblots were carried out with antibodies against SLX4 and XPF.

			n/a: lanes that are not relevant to the colony survival assay. A portion of the corresponding Ponceau stained membrane is shown under the immunoblots. SLX4 runs just above the 250 kDa mark while XPF runs slightly above the 100 kDa mark. (b) Analysis of replication fork dynamics in HeLa cells depleted for SLX4 or RTEL1, as described in Fig. 3a. NT: non-targeting control siRNA. Data are shown in box-plots (median, first and third quartile) with 5th-95th percentile whiskers (+: mean, n: number of unbroken signals analysed). Statistical significance was assessed with the Mann-Whitney test (ns: not significant, ***: $p<0.001$, ****: $p<0.0001$). The immunoblots were performed with antibodies against SLX4, RTEL1 and ß-actin used as internal loading control. The arrow indicates the SLX4 band. (c) as in b in U2OS "Fit0" cells depleted for SLX4 or RTEL1. LUC: control siRNA. (d) Control immunoblots and the corresponding Ponceau stained membrane for Fig. 3b showing the relative levels of endogenous SLX4 (lane 1 before depletion; lanes 2 to 8 after depletion) and recombinant WT or mutated SLX4 proteins expressed in cells depleted for endogenous SLX4 (lanes 3 to 8). SLX4 runs just above the 250 kDa mark while XPF runs slightly above the 100 kDa mark. n/a: lanes that are not relevant to the data shown in Fig. 3b. (e) as in b in U2OS "Fit0" and U2OS Flp-In TREX cells stably expressing DOX-inducible WT or mutated Flag-HA-SLX4 as indicated. $siSLX4^{UTR}$ was used to deplete endogenous SLX4. Uncropped images of the immunoblots in panels a-d and data for graphs in panels a,b,c,e are available as source data.
Extended Data Fig. 6	**SLX4 promotes replication fork progression independently**	NSMB_A41514B_Takedachi_Extended_Data_Fig_6_fi	(a) PLA between SLX4 (HA) and RTEL1 was performed in HeLa Flp-In TREX cells expressing Flag-HA-SLX4 before HA counterstaining (in green and red,

	of its associated SSEs	nal_new.jpg	respectively). PLA spots per HA-positive cells are plotted (red bars: median with interquartile range). Parental HeLa "Fit0" cells were used as a negative control and PLA spots were counted in random nuclei for this condition (grey distribution with orange bars). Kruskal-Wallis test (n>55, ****: p<0.0001). Representative single cells with different HA contents are shown (scale bar: 10 µm). (b) Nascent DNA strands were pulse-labelled with 5-ethynyl-2-deoxyuridine (EdU). Biotin was conjugated to EdU by click chemistry after cell fixation. *In situ* proximity ligation assay (PLA) was performed between endogenous RTEL1 and EdU, using an anti-biotin antibody, before EdU counterstaining (in green and red, respectively). Reactions omitting one of the primary antibodies (Ab) were used as negative controls. The number of PLA spots per EdU-positive cells is plotted, except in the RTEL1 Ab only negative control in which PLA spots were counted in random nuclei (red or orange bars: median with interquartile range, n>79). Statistical significance was tested with the Kruskal-Wallis test (****: p<0.0001). Representative nuclei are shown (scale bar: 10 µm). (c) As in b in SV40-immortalised patient fibroblasts expressing WT or R957W RTEL1. The immunoblot was performed with antibodies against RTEL1 and GAPDH used as internal loading control. Uncropped images of the immunoblots in panel c and data for graphs in panels a-c are available as source data.
Extended Data Fig. 7	**SLX4-RTEL1 interaction is need for tight colocalization between FANCD2 and RNA Pol II and to avoid replication-transcription conflicts**	NSMB_A41514B_Takedachi_Extended_Data_Fig_7_final_new.jpg	(a) Number of SLX4 foci detected by anti-HA immunofluorescence in U2OS Flp-In TREX cells producing the indicated Flag-HA-SLX4 proteins. (b) Representative images of the immunofluorescence data quantified in Fig. 5a and Extended data Fig. 7a. (c) Representative fields for the PLA FANCD2/RNA pol II pS2 shown in Fig. 5c. Scale bar: 10 µm. (d) PLA between SLX4 (HA) and RNA pol II pS2 was performed in U2OS Flp-In

			TREX cells expressing Flag-HA-SLX4 before HA counterstaining. Single-cell HA intensity (n>152, left panel) and PLA spots per HA-positive cells (right panel) are plotted (n>109, red bars: median with interquartile range). Parental U2OS "Fit0" cells were used as a negative control and PLA spots were counted in random nuclei for this condition (grey distribution with orange bars). Kruskal-Wallis test (ns: not significant, ****: p<0.0001). (e) PLA between endogenous RTEL1 and RNA pol II pS2 was performed in SV40-immortalised patient fibroblasts expressing WT or R957W RTEL1. Reactions omitting one of the primary antibodies (Ab) were used as negative controls. Kruskal-Wallis test (ns: not significant, ****: p<0.0001). Data for graphs in panels a,d,e are available as source data.
Extended Data Fig. 8	**Transcription is toxic to replication in absence of SLX4-RTEL1 complex formation**	NSMB_A41514B_Takedachi_Extended_Data_Fig_8_final_new.jpg	a) Supporting data for the DNA fiber assay shown in Fig. 6a. (b) HeLa "Fit0" cells were depleted for SLX4 or RTEL1. 1 µM triptolide was added to the culture medium for 3 h before and during the IdU and CldU pulses to inhibit transcription initiation. Replication fork dynamics was analysed as in Fig. 3a. Mann-Whitney test, ns: not significant, **: p<0.01, ****: p<0.0001). Uncropped images of the immunoblots and data for graphs in panels a and b are available as source data.

1

Item	Present?	Filename This should be the name the file is saved as when it is uploaded to our system, and should include the file extension. The extension must be .pdf	A brief, numerical description of file contents. i.e.: *Supplementary Figures 1-4, Supplementary Discussion, and Supplementary Tables 1-4.*
Supplementary Information	Yes	NSMB_A41514B_Takedachi_Supplementary_Note.pdf	Supplementary note
Reporting Summary	Yes	NSMB_A41514	

		B_nr-reporting-summary.pdf

2

Type	Number If there are multiple files of the same type this should be the numerical indicator. i.e. "1" for Video 1, "2" for Video 2, etc.	Filename This should be the name the file is saved as when it is uploaded to our system, and should include the file extension. i.e.: *Smith_Supplementary_Video_1.mov*	Legend or Descriptive Caption Describe the contents of the file
Supplementary Table	1	NSMB_A41514B_Takedachi_Supplementary_Table_1.xlsx	Full data report from the mass spectrometry analysis of Extended data Fig. 1a
Supplementary Table	2	NSMB_A41514B_Takedachi_Supplementary_Table_2.xlsx	Full data report from the mass spectrometry analysis of Extended data Fig. 1e

3

Figure	Filename This should be the name the file is saved as when it is uploaded to our system, and should include the file extension. i.e.: *Smith_SourceData_Fig1.xls*, or *Smith_Unmodified_Gels_Fig1.pdf*	Data description i.e.: Unprocessed Western Blots and/or gels, Statistical Source Data, etc.
Source Data Fig. 1	NSMB_A41514B_Source_Data_Figure_1.pdf NSMB_A41514B_Takedachi_SourceData_Fig1.xlsx	pdf file: Unprocessed Western Blots and/or gels, FACS data xlsx file: statistical source data and calculation of statistical values
Source Data Fig. 2	NSMB_A41514B_Source_Data_Figure_2.pdf	pdf file: Unprocessed Western Blots and/or gels
Source Data Fig. 3	NSMB_A41514B_Source_Data_Figure_3.pdf NSMB_A41514B_Takedachi_SourceData_Fig3.xlsx	pdf file: Unprocessed Western Blots and/or gels xlsx file: statistical source data and calculation of statistical values
Source Data Fig. 4	NSMB_A41514B_Source_Data_Figure_4.pdf NSMB_A41514B_Takedachi_SourceData_Fig4.xlsx	pdf file: Unprocessed Western Blots and/or gels xlsx file: statistical source data and calculation of statistical values
Source Data Fig. 5	NSMB_A41514B_Source_Data_Figure_5.pdf NSMB_A41514B_Takedachi_SourceData_Fig5.xlsx	pdf file: Unprocessed Western Blots and/or gels xlsx file: statistical source data and calculation of statistical values
Source Data Fig. 6	NSMB_A41514B_Source_Data_Figure_6.pdf	pdf file: Unprocessed Western Blots and/or gels

	NSMB_A41514B_Takedachi_SourceData_Fig6.xlsx	xlsx file: statistical source data and calculation of statistical values
Source Data Extended Data Fig. 1	NSMB_A41514B_Source_Data_Extended_Data_Fig_1.pdf	pdf file: Unprocessed Western Blots and/or gels
Source Data Extended Data Fig. 4	NSMB_A41514B_Source_Data_Extended_Data_Fig_4_new.pdf	pdf file: Unprocessed Western Blots and/or gels
Source Data Extended Data Fig. 5	NSMB_A41514B_Source_Data_Extended_Data_Fig_5_new.pdf NSMB_A41514B_Takedachi_SourceData_ExtData_Fig5_new.xlsx	pdf file: Unprocessed Western Blots and/or gels xlsx file: statistical source data and calculation of statistical values
Source Data Extended Data Fig. 6	NSMB_A41514B_Source_Data_Extended_Data_Fig_6_new.pdf NSMB_A41514B_Takedachi_SourceData_ExtData_Fig6_new.xlsx	pdf file: Unprocessed Western Blots and/or gels xlsx file: statistical source data and calculation of statistical values
Source Data Extended Data Fig. 7	NSMB_A41514B_Takedachi_SourceData_ExtData_Fig7_new.xlsx	
Source Data Extended Data Fig. 8	NSMB_A41514B_Source_Data_Extended_Data_Fig_8_new.pdf NSMB_A41514B_Takedachi_SourceData_ExtData_Fig8_new.xlsx	pdf file: Unprocessed Western Blots and/or gels xlsx file: statistical source data and calculation of statistical values

SLX4 Interacts With RTEL1 To Prevent Transcription-Mediated DNA Replication Perturbations

AUTHOR LIST AND AFFILIATIONS

A. Takedachi[1,2,3§], E. Despras[4§], S. Scaglione[1#], R. Guérois[5#], J.H. Guervilly[1], M. Blin[1], S. Audebert[1], L. Camoin[1], Z. Hasanova[1,6], M. Schertzer[7,8], A. Guille[1], D. Churikov[1], I. Callebaut[9], V. Naim[10], M. Chaffanet[1], J.P. Borg[1], F. Bertucci[1], P. Revy[11], D. Birnbaum[1], A. Londoño-Vallejo[7,8], P.L. Kannouche[4], P.H.L. Gaillard[1*]

[1]Centre de Recherche en Cancérologie de Marseille, CRCM, Inserm, CNRS, Aix-Marseille Université, Institut Paoli-Calmettes, Marseille, France

[2]Inovarion, F-75013 Paris, France

[3]Current address: Department of Chemistry, Faculty of Science, Fukuoka University, Japan

[4]CNRS UMR9019, Université Paris-Saclay, Equipe labellisée Ligue contre le Cancer, Gustave Roussy, Villejuif, France
[5]Institute for Integrative Biology of the Cell (I2BC), CEA, CNRS, Univ. Paris-Sud, Université Paris-Saclay, 91198, Gif-sur-Yvette cedex, France
[6]Current address: Institute of Molecular Genetics, Prague, Czech Republic
[7]Institut Curie, PSL Research University, CNRS, UMR3244, F-75005, Paris, France.
[8]Sorbonne Universités, UPMC Univ Paris 06, CNRS, UMR3244, F-75005, Paris, France.
[9]Sorbonne Université, Muséum National d'Histoire Naturelle, UMR CNRS 7590, IRD, Institut de Minéralogie, de Physique des Matériaux et de Cosmochimie, IMPMC, 75005 Paris, France
[10]CNRS UMR9019, Université Paris-Saclay, Gustave Roussy, Villejuif, France
[11]INSERM Unité Mixte de Recherche (UMR) 1163, Laboratory of Genome Dynamics in the Immune System, Equipe labellisée Ligue contre le Cancer, Paris, France, Paris Descartes–Sorbonne Paris Cité University, Imagine Institute, Paris, France

[§]These authors contributed equally to this work
[#] These authors contributed equally to this work
[*]corresponding author pierre-henri.gaillard@inserm.fr

The SLX4 tumour suppressor is a scaffold that plays a pivotal role in several aspects of genome protection including homologous recombination, interstrand DNA cross-link repair and the maintenance of common fragile sites and telomeres. Here we unravel an unexpected direct interaction between SLX4 and the DNA helicase RTEL1, which until now were viewed as having independent and antagonistic functions. We identify cancer and Hoyeraal-Hreidarsson syndrome-associated mutations in *SLX4* and *RTEL1*, respectively, that abolish SLX4-RTEL1 complex formation. We show that both proteins get recruited to nascent DNA, tightly colocalize with active RNA pol II and that SLX4, in complex with RTEL1, promotes FANCD2/RNA pol II colocalization. Importantly, disrupting SLX4-RTEL1 interaction leads to DNA replication defects in unstressed cells which are rescued by inhibiting transcription. Our data demonstrate that SLX4 and RTEL1 interact to prevent replication-transcription conflicts and provide evidence that this is independent of the nuclease scaffold function of SLX4.

Keywords

SLX4, RTEL1, FANCD2, DNA replication, transcription, cancer, Hoyeraal Hreidarsson syndrome, Fanconi anemia, replication stress, harmonin N-like domain, PAH domain, BTB domain

INTRODUCTION

Multi-protein scaffolds fulfil pivotal functions in the maintenance of genome stability by orchestrating the action of their partners and coordinating mechanisms ranging from DNA damage signalling, cell-cycle control, DNA repair, chromosome segregation to cell division. Amongst these, the human SLX4 (FANCP) tumour suppressor has been in the spotlight since it was found to associate with the XPF-ERCC1, MUS81-EME1 and SLX1 structure-specific endonucleases (SSE) and control these enzymes in interstrand DNA cross-link (ICL) repair, homologous recombination and/or the maintenance of telomeres and common fragile sites[1-11]. SLX4 also associates with other factors involved in the maintenance of genome stability including MSH2, TRF2, TOPBP1 and the PLK1 kinase[1,3,4,12]. Interaction with both ubiquitin and SUMO contributes to the regulatory functions of SLX4[2,7,13], which itself has been shown to promote its own SUMOylation as well as that of its XPF partner[2]. In yeast, Slx4 fulfils additional functions ranging from checkpoint dampening to promoting DNA end resection(for review[14]). The importance of its contribution to such diverse aspects of genome maintenance is underscored by the fact that biallelic mutations in *SLX4* are causative of the rare hereditary syndrome Fanconi anemia that is characterized by chromosomal instability, bone marrow failure, developmental defects and high cancer predisposition[15,16]. Despite the progress made on our understanding of some of SLX4 functions, in particular its well-established prominent role in ICL

repair[1,3,4,13,14,17-19], much remains to be done before we can fully understand the various ways by which SLX4 contributes to the maintenance of genome stability.

Here we unravel an unexpected direct interaction between SLX4 and the RTEL1 helicase, which were viewed until now as having rather independent and antagonistic functions[20]. The RTEL1 helicase contributes to the maintenance of genome stability by facilitating telomere as well as genome-wide replication[20-26]. Its ability to unfold D-loops is believed to reduce crossover rates by promoting double-strand break repair through synthesis-dependent strand annealing[27]. It interacts with PCNA[22] and contributes to the replication of pericentromeric heterochromatin in complex with TRF2[28]. In addition to these DNA-metabolism related functions, which are believed to primarily rely on its helicase activity, RTEL1 is also involved in the trafficking of ribonucleoproteins[29]. The functional importance of RTEL1 is underscored by the fact that biallelic *RTEL1* mutations are associated with Dyskeratosis congenita (DC) and Hoyeraal-Hreidarsson syndrome (HHS), its severe form, characterized by developmental defects, bone marrow failure and immunodeficiency[30,31] while heterozygous *RTEL1* mutations cause pulmonary fibrosis[32,33].

We demonstrate that SLX4 is necessary for optimal DNA replication in unstressed cells and that this relies on its interaction with RTEL1 but not its SSE partners. Importantly, we identify cancer-patient associated *SLX4* and *RTEL1* somatic mutations and HHS-associated *RTEL1* germline mutations that abrogate SLX4-RTEL1 complex formation. We show that both SLX4 and RTEL1 get recruited to nascent DNA strands and that they can be found in the immediate vicinity of active RNA polymerase II (RNA pol II). SLX4 turns out to drive the recruitment and/or accumulation of FANCD2 at RNA pol II. In line with the recently described role of FANCD2 in preventing endogenous transcription-induced replication stress[34,35], we demonstrate that SLX4 and RTEL1 interact to prevent replication-transcription conflicts in unstressed cells.

RESULTS

SLX4 interacts with RTEL1

While conducting tandem mass spectrometry analyses of proteins that co-purify with YFP-SLX4 stably produced in HeLa cells under the control of a doxycycline (Dox)-inducible promoter, we reproducibly and specifically found a small number of RTEL1 peptides in SLX4 complexes (Extended data Fig. 1a, Extended data Fig.2, Supplementary Table 1). Immunoprecipitation and Western blot analysis confirmed SLX4-RTEL1 complex formation and showed that it is not mediated by DNA and is sufficiently robust to be maintained in a high-salt buffer (Fig. 1a). Importantly, endogenous RTEL1 was also detected in pull downs of endogenous SLX4 (Fig. 1b). Furthermore, we found SLX4 and RTEL1 to partially colocalize in the nucleus (Extended data

Fig. 1b) and their interaction, while constitutive throughout the cell cycle, to be enhanced in late-S/G2 and mitosis suggesting a cell-cycle dependent control (Fig. 1c and Extended data Fig. 1c).

SLX4 and RTEL1 are direct binding partners

To map the RTEL1 binding domain in SLX4, we assessed the ability of endogenous RTEL1 to co-immunoprecipitate with various recombinant YFP-tagged fragments of SLX4 produced in HeLa cells (Extended data Fig. 1d). As depicted in Fig. 1d, the RTEL1 binding domain corresponds to a region of SLX4 that encompasses both the BTB domain, which drives the homodimerization of SLX4 and is important for ICL-repair and telomere related functions of SLX4[2,36], and a short conserved amphipathic motif (residues 603 to 626) of unknown function located just upstream of the BTB domain (Fig. 1d and Extended data Fig. 1d). Interestingly, we have identified in biopsied metastases from two unrelated patients (lung metastasis of chondroblastic osteosarcoma and liver metastasis of gastric adenocarcinoma), two somatic mutations that alter conserved residues within that motif (Fig. 1d). Both D614G and L618P mutations abrogate interaction of SLX4 with RTEL1 (Fig. 1e) but not with XPF despite the nearby MLR XPF-binding domain (Fig. 1d). Deletion of the BTB or point mutations in that domain also strongly impairs interaction with RTEL1 (Fig. 1e). Our results indicate that both the short conserved motif upstream of the BTB and the BTB itself are required for optimal interaction with RTEL1. Accordingly, proteomic analyses confirmed that RTEL1 is the primary binding partner of an SLX4 fragment containing the conserved amphipathic motif and the BTB domain (Extended data Fig. 1e, Extended data Fig. 3, Supplementary Table 2). Most strikingly, the D614G and L618P mutations abrogated interaction only with RTEL1, amongst all functionally relevant potential interactors of that region of SLX4 (Extended data Fig. 1e, Extended data Fig. 3, Supplementary Table 2).

Noteworthy, SLX4 and RTEL1 can both interact with TRF2[1,4,8,9,37]. However, SLX4 mutations that abrogate interaction with RTEL1 do not impact interaction with TRF2 and *vice versa* (Fig. 1f). This indicates that TRF2 does not contribute to SLX4-RTEL1 complex formation and suggests that RTEL1 and TRF2, which preferentially associate at the G1/S transition and in S phase[37], bind SLX4 when not in complex with one another.

We next undertook the identification of the SLX4-binding domain in RTEL1. The important contribution of the amphipathic motif in SLX4 provided clues as to which part of RTEL1 might be involved in the SLX4-RTEL1 interaction. Indeed, RTEL1 contains two harmonin-N-like motifs that are related to the paired amphipathic helix (PAH) domain[38]. The PAH domain is a protein-protein interaction module that folds into a helical bundle structure that forms a hydrophobic cleft for the binding of a short amphipathic helix. Such a helix is predicted to form between residues 604 and 620 within the conserved domain of SLX4 that is critical for binding to RTEL1 (Fig. 1d). Our modelling analyses suggested that both harmonins of RTEL1 could accommodate

this helix (Fig. 2a). In particular, residues D614 and L618 in SLX4 would lie at the interface of the helix and the harmonins-binding site. Supporting our prediction, an RTEL1$^{763-1164}$ fragment that contains both harmonin domains (HD) efficiently pulls down endogenous SLX4 (Fig. 2b). Direct interaction between SLX4 and RTEL1 and precise mapping of the SLX4-binding domain in RTEL1 were further monitored by yeast two hybrid (Y2H). Interestingly, the amphipathic helix and the BTB are jointly needed to interact with an RTEL1 fragment containing both HDs as no interaction was detected with just the helix (Fig. 2c). In contrast to our modelling predictions (Fig. 2a), interaction was detected only with the first HD (HD1) (Fig. 2c). This specificity turned out to rely on a short conserved sequence located just after the C-terminus of HD1 that is not found after the second harmonin domain (HD2) as an HD1 fragment lacking this short sequence, does not bind SLX4 (Fig. 2c and Extended data Fig. 4a). Both SLX4 D614G and L618P patient-derived mutations totally abrogate interaction with RTEL1 in Y2H (Fig. 2d), confirming that the conserved amphipathic motif of SLX4 is essential for direct binding to RTEL1. The specificity of this direct interaction was further confirmed *in vitro* with bacterially produced recombinant SLX4 and RTEL1 fragments (Figure 2e and Extended data Fig. 4b). Interestingly, amongst the *RTEL1* germline mutations identified in HHS patients, four missense mutations have been mapped within HD1 and two nonsense mutations in the non-structured segment that links HD1 and HD2[38]. Strikingly, all six mutations negatively impact interaction with SLX4 (Fig. 2f-h and Extended data Fig. 4c,d). Our findings demonstrate that SLX4 and RTEL1 are direct binding partners and suggest a complex mode of interaction that strictly relies on not only the docking of a conserved amphipathic helix of SLX4 with the first HD of RTEL1 but also on the BTB homo-dimerization domain of SLX4.

SLX4 promotes replication fork progression and genome stability via interaction with RTEL1

Having established that SLX4 and RTEL1 are direct binding partners, we next sought to understand the functional relevance of this interaction. Overall, both proteins are required for many of the same genome maintenance aspects including control of telomere homeostasis, ICL repair and homologous recombination. However, it is not known whether they act within the same pathways and, at least in mice, they have rather independent and antagonistic functions at telomeres where RTEL1 unfolds T-loops to prevent their SLX4-driven endonucleolytic processing and telomere attrition[20]. Considering our findings, one explanation could have been that RTEL1 also prevents such unscheduled processing of secondary DNA structures at telomeres by directly interacting with SLX4 and negatively controlling its associated structure-specific endonucleases (SSEs). However, we observed no telomere attrition in human cells producing the RTEL1-binding defective SLX4^{D614G} and SLX4^{L618P} mutants, arguing against such a scenario (data not shown). We also did not observe any increased cellular sensitivity to

mitomycin C in those cells indicating that SLX4 and RTEL1 do not need to interact to fulfil their functions in ICL repair (Extended data Fig. 5a).

RTEL1 plays a role in genome wide replication through direct interaction with PCNA[22]. Accordingly, impaired replication is observed in mouse cells expressing a PCNA-binding defective mutant[22] or following depletion of RTEL1 in human cells[22,28]. Since SLX4 can also be found associated with the replisome[39], we first assessed in DNA fiber assays whether loss of SLX4 similarly impairs replication. Cells were transfected with different siRNAs targeting SLX4 or control siRNAs and nascent DNA was labelled *in vivo* by successive pulses of iododeoxyuridine (IdU) and chlorodeoxyuridine (CldU). Analogues and total DNA were detected by immunofluorescence on spread DNA molecules. Depletion of SLX4 in HeLa and U2OS cells resulted in shorter nascent DNA tracks and increased fork ratio. This is indicative of impaired replication fork progression, as seen following depletion of RTEL1[28] (Fig. 3a and Extended data Fig. 5b,c). Importantly, the replication defects caused by depletion of SLX4 were fully rescued by the expression of Flag-HA-SLX4^{WT} but not Flag-HA-SLX4^{D614G} or Flag-HA-SLX4^{L618P} (Fig. 3b and Extended data Fig. 5d,e). Using *in situ* proximity ligation assays (PLA) between SLX4 and neo-synthesized DNA or RTEL1, we found that SLX4 does not need to interact with RTEL1 to get recruited to the replication fork (Fig. 3c) and that both proteins do not need to interact to get recruited in the vicinity of one another (Extended data Fig. 6a). To confirm that SLX4-RTEL1 complex formation is nevertheless critical for proper replication fork progression in unchallenged cells, we used an HHS patient-derived immortalized cell line (P7) carrying a homozygous missense R957W mutation in HD1[31] that abrogates binding to SLX4 (Fig. 2f,g and Extended data Fig. 4d). Although RTEL1^{R957W}, which has an intact PCNA interacting motif (PIP), is recruited like RTEL1^{WT} to neo-synthesized DNA (Extended data Fig. 6b,c), the P7 patient-derived cell line presented short nascent DNA tracks and a high fork ratio (Fig. 3d), reminiscent of what we observed in cells producing SLX4 mutants that cannot bind RTEL1 (Fig. 3b and Extended data Fig. 5d,e).

Overall our results demonstrate that SLX4 is necessary for proper replication in unchallenged cells and that it must associate with RTEL1 to help the replisome overcome situations which impede replication fork progression during normal S-phase.

SLX4 prevents replication perturbations independently of its associated structure-specific endonucleases

Both MUS81 and XPF-ERCC1 were shown to promote normal replication fork rates during unperturbed S phase[40]. To assess whether the RTEL1-dependent function of SLX4 in DNA replication in unstressed cells relies or not on its interaction with its associated SSEs, we generated an SLX4^{-SMX} mutant that is unable to interact with all three SSE partners (Fig. 4a). This mutant carries a combination of *SLX4* mutations that were previously shown to each

abrogate interaction between SLX4 and one of its SSE partners[2,41]. Immunoprecipitation of DOX-inducible Flag-HA-SLX4^{-SMX} stably expressed in HeLa Flp-In TREX cells confirmed severely impaired interactions with all three SSE partners (Fig. 4b). Remarkably though and in stark contrast to the RTEL1-binding defective mutants, the SLX4^{-SMX} mutant fully rescued the replication defects caused by depletion of endogenous SLX4 (Fig. 4c). This demonstrates that in unstressed cells SLX4 acts with RTEL1 to promote replication fork progression independently of its associated SSEs.

SLX4 promotes FANCD2 foci formation via interaction with RTEL1

The Fanconi anemia pathway protein FANCD2 ensures proper replication fork progression in response to various endogenous and exogenous sources of replication impediments (for review[42]). In unchallenged cells, FANCD2 is monoubiquitinated and can form spontaneous foci[43]. Interestingly, we noticed that depletion of SLX4 induced a drop in the amount of spontaneous FANCD2 foci (Fig. 5a) without altering the level of monoubiquitination of FANCD2 (data not shown). This was fully rescued by expression of Flag-HA-SLX4^{WT} but not Flag-HA-SLX4^{D614G} or Flag-HA-SLX4^{L618P} (Fig. 5a and Extended data Fig. 7a,b). Our results demonstrate that SLX4 drives the formation of FANCD2 foci in unchallenged cells and that this relies on its interaction with RTEL1. FANCD2 was recently shown to colocalize with RNA polymerase II (RNA pol II) and contributes to preventing endogenous transcription-induced replication stress[34,35]. We thus assessed whether SLX4 may influence the recruitment and/or persistence of FANCD2 in the vicinity of active RNA pol II. We observed a reduction in proximity ligation assay (PLA) signals between FANCD2 and phosphorylated RNA pol II upon depletion of SLX4 (Fig. 5b). This was rescued by SLX4^{WT} but not the RTEL1-binding defective mutants (Fig. 5c and Extended data Fig. 7c), indicating that the accumulation of FANCD2 in the vicinity of active RNA pol II requires an interaction between SLX4 and RTEL1.

SLX4 binds RTEL1 to prevent conflicts between replication and transcription

Since SLX4 appeared to drive the association of FANCD2 with RNA pol II we hypothesized that it might itself be found in the immediate vicinity of RNA pol II. As shown in Fig. 5d, SLX4 can be found in association with RNA pol II in PLA analyses. This was also the case for RTEL1 (Fig. 5e). However, as observed for the association of SLX4 and RTEL1 with nascent DNA, RTEL1-binding defective SLX4^{D614G} and SLX4^{L618P} mutants were also detected in the vicinity of RNA pol II indicating that SLX4 does not need to associate with RTEL1 to reach RNA pol II (Extended data Fig. 7d). Similarly, we also found the SLX4-binding defective RTEL1^{R957W} mutant to be in tight vicinity with RNA Pol II in the P7 patient-derived cell line (Extended data Fig. 7e). Although we cannot exclude that the pools of SLX4 and RTEL1 that we find associated with nascent DNA strands (Fig. 3c and Extended data Fig. 6b,c) are different from those associated with active

RNA pol II (Fig. 5d,e and Extended data Fig. 7d,e), it is tempting to speculate that SLX4 and RTEL1 play a role at the interface of DNA replication and transcription where they help replication overcome transcription-mediated impediments. To test this hypothesis we used PLA to determine whether depletion of SLX4 or RTEL1 leads to increased colocalization between PCNA and active RNA pol II, which has been used as a readout of collisions between DNA replication and transcription[44]. In agreement, a significant increase of PCNA tightly colocalized with RNA pol II was detected in SLX4 and RTEL1-depleted cells compared to mock depleted cells (Fig. 5f).

Finally, to determine if transcription is responsible for the replication defects seen in cells lacking SLX4 and RTEL1 we tested the impact of transcription inhibition on replication fork dynamics. Strikingly, inhibiting transcription with cordycepin or triptolide rescued the replication defects caused by depletion of SLX4 or RTEL1 (Fig. 6a and Extended data Figure 8a,b). It also corrected those resulting from loss of SLX4-RTEL1 complex formation in cells producing the RTEL1-binding defective SLX4^{D614G} or SLX4^{L618P} mutants and in the P7 patient-derived cell line that produces the SLX4-binding defective RTEL1^{R957W} mutant (Fig. 6b,c). Overall our results demonstrate that SLX4 and RTEL1 play a key role in preventing replication impediments caused by transcription which relies on their direct interaction.

DISCUSSION

We have unravelled a direct interaction between SLX4 and RTEL1 and demonstrated that this interaction is critical to help DNA replication overcome transcription-mediated impediments. By showing that the SLX4-RTEL1 interaction is mediated through the association of a conserved amphipathic helix and the BTB domain of SLX4 with the HD1 of RTEL1, we assign a function to a highly conserved region of SLX4 that was of unknown function until now and identify the first partner of one of the HDs of RTEL1, which has important implications in terms of human disease as later discussed. We also assign a possibly novel function to the BTB domain, which was previously shown to mediate homodimerization of SLX4[2,36]. The fact that the interaction between the amphipathic helix of SLX4 and the HD1 of RTEL1 is not sufficient for stable SLX4-RTEL1 interaction, which also relies on the BTB domain of SLX4, suggests a more elaborate mode of interaction than the canonical interaction that is established between a harmonin-like PAH domain in SIN3 and an amphipathic helix in MAD1[45,46]. Instead, the contribution made by the BTB domain of SLX4 is closer to what has been described for the interaction between CCM2 and MEKK3 where the interaction between an amphipathic helix in MEKK3 with the harmonin homology domain of CCM2 is stabilized by the PB1 protein binding domain of MEKK3[47]. Structural analyses will help to better characterize the SLX4-RTEL1 binding interface and determine whether dimerization *per se* is necessary for binding to RTEL1

296 and/or whether the BTB domain makes direct contacts with RTEL1. Such analyses should also
297 provide insight into how the association between SLX4 and RTEL1 might be controlled.
298 Adding to the multiple roles that SLX4 fulfils in the maintenance of genome stability (for review
299 see[14]), we demonstrate that SLX4 contributes to genome wide DNA replication in unstressed
300 cells and that this relies on its direct interaction with RTEL1 (Fig. 3), since $SLX4^{D614G}$ and
301 $SLX4^{L618P}$ mutants that cannot bind RTEL1 are unable to rescue the replication defects caused
302 by depletion of endogenous SLX4. We cannot fully exclude that the D614G and L618P
303 mutations might impact additional functionalities of SLX4. However, both mutations affect highly
304 conserved residues within the amphipathic helix of SLX4 that are ideally positioned to engage in
305 contacts with the harmonins of RTEL1 (Fig. 2) and they are not predicted to impact the overall
306 fold of SLX4. Furthermore, we identified RTEL1 as the only functionally relevant interactor of
307 SLX4 to be impacted by both mutations (Extended data Fig. 1e, Extended data Fig. 3,
308 Supplementary Table 2) and, last but not least, an HHS patient-derived cell line producing an
309 RTEL1 mutant that cannot bind SLX4 (Fig. 2f,g and Extended data Fig. 4d) phenocopies the
310 replication defects of cells producing the $SLX4^{D614G}$ and $SLX4^{L618P}$ mutants (Fig. 3b and 3d,
311 Extended data Fig. 5d,e). Therefore, all evidence points towards a need for SLX4 to interact
312 with RTEL1 to facilitate replication genome wide. Quite remarkably though, we find that it does
313 not need to interact with its SSE partners (Fig. 4), providing unprecedented evidence of a
314 function of SLX4 in human cells that is totally independent of its established nuclease scaffold
315 functions. Our findings further demonstrate that the SLX4-RTEL1 complex is necessary to
316 prevent replication-transcription conflicts (Fig. 5, 6). Indeed, inhibiting transcription not only
317 compensated for the loss of SLX4 or RTEL1, it alleviated to the same extent the replication
318 defects that result from impaired SLX4-RTEL1 complex formation (Fig. 6 and Extended data Fig.
319 8). Noteworthy, those replication defects were monitored through unbiased DNA fiber analyses
320 in unstressed cells. Therefore, the transcription-mediated impairments to DNA replication seen
321 in absence of SLX4 or RTEL1 must be frequent enough to be detected by such genome wide
322 analyses and not restricted to a limited number of loci.
323 Interestingly, RTEL1 was recently found to contribute to the removal of protein-DNA
324 complexes that hinder the progression of replication forks[48]. Therefore, one way by which the
325 SLX4-RTEL1 complex may circumvent replication-transcription conflicts could be by promoting
326 the clearance of the RNA polymerase complex in the vicinity of replication forks. However, given
327 the functional ties between both RTEL1 and SLX4 and the processing of secondary DNA
328 structures, it is likely that the SLX4-RTEL1 complex is involved in non-nucleolytic processing of
329 nucleic acid structures that form as a result of replication-transcription conflicts. Amongst these,
330 R-loops that consist of a DNA:RNA hybrid and a displaced single-stranded DNA loop, which
331 itself can form G-quadruplexes that stabilize the R-loop[49], represent a major obstruction for
332 replication fork progression[50]. In line with a role in R-loop processing, we find that SLX4 drives

333 the accumulation and/or stabilization of FANCD2 in the direct vicinity of RNA pol II (Fig. 5b,c).
334 FANCD2, along with other components of the Fanconi anemia pathway, makes important
335 contributions to the signalling of R-loops and their processing[34,35,44,51]. Intriguingly, we found that
336 SLX4 and RTEL1 can be detected in close proximity to one another, even when they cannot
337 interact, and are independently recruited to nascent DNA and RNA pol II (Fig. 3c and Extended
338 data Fig. 6). Yet, SLX4-RTEL1 complex formation is required for the tight colocalization of
339 FANCD2 and RNA pol II and is essential for proper replication fork progression (Fig. 3b,d,
340 Extended data Fig. 5e and Fig. 7c). This suggests that both proteins get recruited independently
341 from one another but that they need at one stage to make contact for replication to proceed
342 normally. Such contact may constitute a molecular switch that allows SLX4 to control the
343 catalytic activity of the RTEL1 helicase for the timely processing of secondary structures that
344 impede replication fork progression.

345 Although we found the SLX4-RTEL1 interaction to be constitutive throughout the cell
346 cycle, we noticed that it increased in late S and G2/M phases (Fig. 1c). Noteworthy, both
347 FANCD2 and SLX4 contribute to the maintenance of common fragile sites (CFS) in late G2 and
348 mitosis[2,6,52,53]. Furthermore, R-loops have been found to accumulate at CFS in absence of
349 FANCD2[51,54]. Therefore, the preferential interaction between SLX4 and RTEL1 in late S/G2 may
350 reflect an additional and specific role related to the maintenance of CFS and/or other late
351 replicating loci where SLX4 recruits RTEL1 for the processing of G4-associated R-loops as
352 recently described[55].

353 The relevance of our findings in terms of human disease is underscored by the
354 identification of cancer-derived somatic *SLX4* mutations and HHS-associated germline *RTEL1*
355 mutations that abrogate the SLX4-RTEL1 interaction (Fig. 1d,e and 2d-h). It is striking that *de*
356 *novo* mutations, each impacting a different and highly conserved residue in the predicted
357 amphipathic helix of SLX4 and that abrogate interaction with RTEL1, were identified in two
358 unrelated patients presenting different disease profiles. Furthermore, the HHS-associated
359 germline homozygote R957W mutation in the HD1 of RTEL1, is also reported in the COSMIC
360 data base[56] as the most represented cancer-associated somatic mutation identified in *RTEL1*.
361 Considering that replication stress is an established hallmarks of tumorigenesis (for review[57]
362 and that loss of interaction between SLX4 and RTEL1 perturbs DNA replication (Fig. 3b and
363 Extended data Fig. 5e), it is tempting to speculate that mutations in SLX4 and RTEL1 that
364 abrogate complex formation are more than just passenger mutations. Replication-transcription
365 conflicts, which have been linked to the fragility of both late and early-replicating fragile sites of
366 the genome[58-60], are emerging as a potentially much broader source of genome instability with
367 the realization that transcription is a pervasive process that covers more than 80% of the human
368 genome[61,62]. Moreover, oncogene activation during tumorigenesis drives premature entry into S
369 phase and the firing of intragenic origins, which increases conflicts between replication and

transcription and genomic instability[63]. Thus, it will be important to assess what impact *SLX4* and *RTEL1* mutations that abrogate SLX4-RTEL1 complex formation have on the tumoral process. Importantly, we have also shown that all reported HHS-associated germline mutations mapped in the HD1 of RTEL1 negatively impact interaction with SLX4, suggesting that loss of SLX4-RTEL1 complex formation contributes to the aetiology of the disease. We cannot at this stage draw any conclusions as to whether *SLX4* mutations that abrogate SLX4-RTEL1 complex formation could be associated with HHS, since both D614G and L618P SLX4 variants that we have identified in cancer patients were somatic mutations with low allelic frequencies. Furthermore, bi-allelic germline mutations in *SLX4* have been associated until now with Fanconi anemia[15,16]. However, there are many cases where different mutations in the same gene are associated with different pathologic outcomes and diseases. Therefore, it will be important to determine what clinical phenotypes might be associated with germline *SLX4* mutations that abrogate SLX4-RTEL1 complex formation and whether *SLX4* should be considered as a possible candidate gene for HHS.

Our demonstration of a functionally relevant interaction between SLX4 and RTEL1 redefines the way we ought to think about how they contribute to the maintenance of genome stability and opens new lines of investigation to help better understand how they prevent the emergence of cancer and other human diseases.

ACKNOWLEDGEMENTS

A.T. and P.-H.G. express their gratitude to Micaela Boiero Sanders and Christophe Machu for their help in the analysis of microscopy data. The authors thank Mauro Modesti for supplying the GFP nanobody and all members of the 3R community of the CRCM for helpful discussions. They also thank Samuel Granjeaud for helpful discussions on statistical analyses.

Work in the laboratory of P.H.L.G. was funded by Institut National du Cancer (INCa-PLBio2016-159), Siric-Cancéropôle PACA (AAP Projets émergents 2015). A.T. was supported by (INCa-PLBio2016-159), Z.H. was supported by (INCa-PLBio2016-159) and Fondation ARC. Work in the laboratory of D.B. was funded by SIRIC (INCa-DGOS-Inserm 6038), Label Ligue (EL2016 DB), Ruban Rose and Fondation Groupe EDF. The laboratory of P.K. was supported by INCa (INCa-PLBio2016-159) and INCa-DGOS-Inserm 12551, E.D. was supported by INCa (PLBio2016-144). V.N.'s research is supported by the ERC starting grant agreement # 638898. Work in the laboratory of R.G. was funded by FRISBI (ANR-10-INSB-05-01) and ANR CHIPSET (ANR-15-CE11-0008-01). RTEL1 related work in ALV, PR and IC laboratories was partially supported by a joint grant from the Agence Nationale pour la Recherche (ANR-14-CE10-0006-01). The IBiSA Marseille Proteomic platform is funded by Institut Paoli-Calmettes, National Institute of Cancer and Aix-Marseille University. J.P.B. is a scholar of Institut Universitaire de France.

We wish to thank Dr Liu and Dr Hickson for sharing unpublished results.

AUTHOR CONTRIBUTIONS

A.T. performed experiments for proteomic analyses, biochemical analyses of the SLX4-RTEL1 interaction, colony survival assays and the analysis of FANCD2 foci formation. A.T. generated all cell lines producing YPF- or Flag-HA-tagged recombinant proteins used in the current study. E.D. performed all DNA fiber analyses and PLA experiments. S.S. generated plasmids used in Y2H and designed and performed all Y2H experiments. R.G. performed all structural analyses with the help of I.C. and helped in the design of *in vitro* biochemical studies. J.H.G. worked on the detection of the endogenous SLX4-RTEL1 complex, generated reagents and helped with data analysis. M.B. performed the pulldowns and characterization of Flag-HA-SLX4^{-SMX}. S.A. and L.C. carried out all proteomic analyses, with insight and expertise from J.P.B.. A.G., M.C., F.B. and D.B. ran the NGS of biological samples and bioinformatic analyses of the *SLX4* patient derived mutations. P.R. generated the fibroblast cell line from the RTEL1-deficient patient P7 and helped in the design and data interpretation of experiments with HHS-associated *RTEL1* mutations. Z.H., D.C., and V.N. helped in the design of cellular studies and data analysis. M.S. and A.L-V. generated the RTEL1 antibody and contributed to the design of experiments and data interpretation. P.H.G. produced recombinant proteins and performed *in vitro* binding assays and wrote the manuscript. The manuscript was reviewed by all authors. A.T., E.D., P.K. and P.H.G. conceived and planned the study.

Correspondence and requests for materials should be addressed to P.H.L.G.

COMPETING INTEREST STATEMENT

The authors declare no competing interests.

REFERENCES

1. Fekairi, S. *et al.* Human SLX4 is a Holliday junction resolvase subunit that binds multiple DNA repair/recombination endonucleases. *Cell* **138,** 78–89 (2009).
2. Guervilly, J.-H. *et al.* The SLX4 complex is a SUMO E3 ligase that impacts on replication stress outcome and genome stability. *Mol. Cell* **57,** 123–137 (2015).
3. Munoz, I. M. *et al.* Coordination of structure-specific nucleases by human SLX4/BTBD12 is required for DNA repair. *Mol. Cell* **35,** 116–127 (2009).
4. Svendsen, J. M. *et al.* Mammalian BTBD12/SLX4 assembles a Holliday junction resolvase and is required for DNA repair. *Cell* **138,** 63–77 (2009).
5. Andersen, S. L. *et al.* Drosophila MUS312 and the vertebrate ortholog BTBD12 interact with DNA structure-specific endonucleases in DNA repair and recombination. *Mol. Cell* **35,** 128–135 (2009).
6. Minocherhomji, S. *et al.* Replication stress activates DNA repair synthesis in mitosis. *Nature* **528,** 286–290 (2015).
7. Ouyang, J. *et al.* Noncovalent interactions with SUMO and ubiquitin orchestrate distinct functions of the SLX4 complex in genome maintenance. *Mol. Cell* **57,** 108–122 (2015).
8. Wilson, J. S. J. *et al.* Localization-Dependent and -Independent Roles of SLX4 in Regulating Telomeres. *Cell Rep* **4,** 853–860 (2013).
9. Wan, B. *et al.* SLX4 Assembles a Telomere Maintenance Toolkit by Bridging Multiple Endonucleases with Telomeres. *Cell Rep* **4,** 861–869 (2013).
10. Wyatt, H. D. M., Sarbajna, S., Matos, J. & West, S. C. Coordinated Actions of SLX1-SLX4 and MUS81-EME1 for Holliday Junction Resolution in Human Cells. *Mol. Cell* **52,** 1–14 (2013).
11. Duda, H. *et al.* A Mechanism for Controlled Breakage of Under- replicated Chromosomes during Mitosis. *Dev. Cell* **39,** 740–755 (2016).
12. Gritenaite, D. *et al.* A cell cycle-regulated Slx4-Dpb11 complex promotes the resolution of DNA repair intermediates linked to stalled replication. *Genes Dev* **28,** 1604–1619 (2014).
13. Kim, Y. *et al.* Regulation of multiple DNA repair pathways by the Fanconi anemia protein SLX4. *Blood* **121,** 54–63 (2013).
14. Guervilly, J.-H. & Gaillard, P.-H. SLX4: multitasking to maintain genome stability. *Critical Reviews in Biochemistry and Molecular Biology* **53,** 475–514 (2018).
15. Stoepker, C. *et al.* SLX4, a coordinator of structure-specific endonucleases, is mutated in a new Fanconi anemia subtype. *Nat Genet* **43,** 138–141 (2011).
16. Kim, Y. *et al.* Mutations of the SLX4 gene in Fanconi anemia. *Nat Genet* **43,** 142–146 (2011).
17. Douwel, D. K. *et al.* XPF-ERCC1 Acts in Unhooking DNA Interstrand Crosslinks in Cooperation with FANCD2 and FANCP/SLX4. *Mol. Cell* **54,** 1–12 (2014).
18. Hodskinson, M. R. G. *et al.* Mouse SLX4 is a tumor suppressor that stimulates the activity of the nuclease XPF-ERCC1 in DNA crosslink repair. *Mol. Cell* **54,** 472–484 (2014).
19. Lachaud, C. *et al.* Distinct functional roles for the two SLX4 ubiquitin-binding UBZ domains mutated in Fanconi anemia. *J Cell Sci* **127,** 2811–2817 (2014).
20. Vannier, J.-B., Pavicic-Kaltenbrunner, V., Petalcorin, M. I. R., Ding, H. & Boulton, S. J. RTEL1 dismantles T loops and counteracts telomeric G4-DNA to maintain telomere integrity. *Cell* **149,** 795–806 (2012).
21. Ding, H. *et al.* Regulation of murine telomere length by Rtel: an essential gene encoding a helicase-like protein. *Cell* **117,** 873–886 (2004).
22. Vannier, J.-B. *et al.* RTEL1 is a replisome-associated helicase that promotes telomere and genome-wide replication. *Science* **342,** 239–242 (2013).
23. Uringa, E.-J. *et al.* RTEL1 contributes to DNA replication and repair and telomere maintenance. *Mol Biol Cell* **23,** 2782–2792 (2012).
24. Sfeir, A. *et al.* Mammalian telomeres resemble fragile sites and require TRF1 for efficient replication. *Cell* **138,** 90–103 (2009).

25. Sarek, G., Vannier, J.-B., Panier, S., Petrini, J. H. J. & Boulton, S. J. TRF2 Recruits RTEL1 to Telomeres in S Phase to Promote T-Loop Unwinding. *Mol. Cell* **61,** 788–789 (2016).
26. Porreca, R. M. *et al.* Human RTEL1 stabilizes long G-overhangs allowing telomerase-dependent over-extension. *Nucleic Acids Res* **46,** 4533–4545 (2018).
27. Youds, J. L. *et al.* RTEL-1 enforces meiotic crossover interference and homeostasis. *Science* **327,** 1254–1258 (2010).
28. Mendez-Bermudez, A. *et al.* Genome-wide Control of Heterochromatin Replication by the Telomere Capping Protein TRF2. *Mol. Cell* **70,** 449–461.e5 (2018).
29. Schertzer, M. *et al.* Human regulator of telomere elongation helicase 1 (RTEL1) is required for the nuclear and cytoplasmic trafficking of pre-U2 RNA. *Nucleic Acids Res* **43,** 1834–1847 (2015).
30. Ballew, B. J. *et al.* A recessive founder mutation in regulator of telomere elongation helicase 1, RTEL1, underlies severe immunodeficiency and features of Hoyeraal Hreidarsson syndrome. *PLoS Genet* **9,** e1003695 (2013).
31. Touzot, F. *et al.* Extended clinical and genetic spectrum associated with biallelic RTEL1 mutations. *Blood Adv* **1,** 36–46 (2016).
32. Cogan, J. D. *et al.* Rare variants in RTEL1 are associated with familial interstitial pneumonia. *Am. J. Respir. Crit. Care Med.* **191,** 646–655 (2015).
33. Kannengiesser, C. *et al.* Heterozygous RTEL1 mutations are associated with familial pulmonary fibrosis. *Eur. Respir. J.* **46,** 474–485 (2015).
34. Schwab, R. A. *et al.* The Fanconi Anemia Pathway Maintains Genome Stability by Coordinating Replication and Transcription. *Mol. Cell* **60,** 351–361 (2015).
35. García-Rubio, M. L. *et al.* The Fanconi Anemia Pathway Protects Genome Integrity from R-loops. *PLoS Genet* **11,** e1005674 (2015).
36. Yin, J. *et al.* Dimerization of SLX4 contributes to functioning of the SLX4-nuclease complex. *Nucleic Acids Res* **44,** gkw354–4880 (2016).
37. Sarek, G., Vannier, J.-B., Panier, S., Petrini, J. H. J. & Boulton, S. J. TRF2 recruits RTEL1 to telomeres in S phase to promote t-loop unwinding. *Mol Cell* ***57*****,** 622–635 (2015).
38. Faure, G., Revy, P., Schertzer, M., Londoño-Vallejo, A. & Callebaut, I. The C-terminal extension of human RTEL1, mutated in Hoyeraal-Hreidarsson syndrome, contains harmonin-N-like domains. *Proteins* **82,** 897–903 (2014).
39. Dungrawala, H. *et al.* The Replication Checkpoint Prevents Two Types of Fork Collapse without Regulating Replisome Stability. *Mol Cell* **59,** 1–14 (2015).
40. Fu, H. *et al.* The DNA repair endonuclease Mus81 facilitates fast DNA replication in the absence of exogenous damage. *Nat Commun* **6,** 6746–14 (2015).
41. Castor, D. *et al.* Cooperative Control of Holliday Junction Resolution and DNA Repair by the SLX1 and MUS81-EME1 Nucleases. **52,** 1–13 (2013).
42. Federico, M. B., Campodónico, P., Paviolo, N. S. & Gottifredi, V. Beyond interstrand crosslinks repair: contribution of FANCD2 and other Fanconi Anemia proteins to the replication of DNA. *Mutat Res* **808,** 83–92 (2018).
43. Taniguchi, T. *et al.* S-phase-specific interaction of the Fanconi anemia protein, FANCD2, with BRCA1 and RAD51. *Blood* **100,** 2414–2420 (2002).
44. Okamoto, Y. *et al.* FANCD2 protects genome stability by recruiting RNA processing enzymes to resolve R-loops during mild replication stress. *FEBS J.* **668,** 4 (2018).
45. Brubaker, K. *et al.* Solution structure of the interacting domains of the Mad-Sin3 complex: implications for recruitment of a chromatin-modifying complex. *Cell* **103,** 655–665 (2000).
46. Spronk, C. A. *et al.* The Mad1-Sin3B interaction involves a novel helical fold. *Nat. Struct. Biol.* **7,** 1100–1104 (2000).
47. Fisher, O. S. *et al.* Structure and vascular function of MEKK3–cerebral cavernous malformations 2 complex. *Nat Commun* **6,** 1–11 (1AD).
48. Sparks, J. L. *et al.* The CMG Helicase Bypasses DNA-Protein Cross-Links to Facilitate Their Repair. *Cell* **176,** 167–181.e21 (2019).

49. De Magis, A. *et al.* DNA damage and genome instability by G-quadruplex ligands are mediated by R loops in human cancer cells. *Proceedings of the National Academy of Sciences* **116,** 816–825 (2019).
50. Bhatia, V. *et al.* BRCA2 prevents R-loop accumulation and associates with TREX-2 mRNA export factor PCID2. *Nature* **511,** 362–365 (2014).
51. Okamoto, Y. *et al.* Replication stress induces accumulation of FANCD2 at central region of large fragile genes. *Nucleic Acids Res* **46,** 2932–2944 (2018).
52. Chan, K. L., Palmai-Pallag, T., Ying, S. & Hickson, I. D. Replication stress induces sister-chromatid bridging at fragile site loci in mitosis. *Nat Cell Biol* **11,** 753–760 (2009).
53. Naim, V. & Rosselli, F. The FANC pathway and BLM collaborate during mitosis to prevent micro-nucleation and chromosome abnormalities. *Nat Cell Biol* **11,** 761–768 (2009).
54. Madireddy, A. *et al.* FANCD2 Facilitates Replication through Common Fragile Sites. *Mol. Cell* **64,** 388–404 (2016).
55. Wu, W. RTEL1 suppresses G-quadruplex-associated R-loops at difficult-to-replicate loci in the human genome. *Nature structural molecular biology* 1–2 (2020).
56. Tate, J. G. *et al.* COSMIC: the Catalogue Of Somatic Mutations In Cancer. *Nucleic Acids Res* **47,** D941–D947 (2018).
57. Macheret, M. & Halazonetis, T. D. DNA replication stress as a hallmark of cancer. *Annu Rev Pathol* **10,** 425–448 (2015).
58. Helmrich, A., Ballarino, M. & Tora, L. Collisions between replication and transcription complexes cause common fragile site instability at the longest human genes. *Mol. Cell* **44,** 966–977 (2011).
59. Blin, M. *et al.* Transcription-dependent regulation of replication dynamics modulates genome stability. *Nat Struct Mol Biol* **26,** 58–66 (2019).
60. Barlow, J. H. *et al.* Identification of early replicating fragile sites that contribute to genome instability. *Cell* **152,** 620–632 (2013).
61. Hangauer, M. J., Vaughn, I. W. & McManus, M. T. Pervasive transcription of the human genome produces thousands of previously unidentified long intergenic noncoding RNAs. *PLoS Genet* **9,** e1003569 (2013).
62. Djebali, S. *et al.* Landscape of transcription in human cells. *Nature* **489,** 101–108 (2012).
63. Macheret, M. & Halazonetis, T. D. Intragenic origins due to short G1 phases underlie oncogene-induced DNA replication stress. *Nature* **555,** 112–116 (2018).

FIGURE LEGENDS

Fig. 1: SLX4 interacts with RTEL1

(a) YFP-pull down from HeLa cells expressing YFP-SLX4. In lanes 3- 5, YFP-pull downs were washed in a high salt buffer (NaCl) or carried out in the presence of Benzonase (Benzo) or Ethidium bromide (EtBr) as indicated. MUS81 and XPF were used as positive controls for SLX4-binding.

(b) Endogenous SLX4 was immunoprecipitated from a HeLa cell-lysate with a combination of two different anti-SLX4 and visualized by western blotting.

(c) Immunoprecipitation of Flag-HA-SLX4 from dox-inducible HeLa cells at the indicated time points after release from a thymidine block. Cell cycle profiles of the samples are shown at left. Immunoblot of a representative experiment (right) and the quantifications of n=3 independent experiments. Error bars = mean ± s.e.m.

(d) Schematic diagram showing RTEL1-binding domain of SLX4, and multiple SLX4 sequence alignment centred on the region 599-635 of human SLX4. Top two sequences report secondary structures (H: helix) and disorder status (D) predicted by PSIPRED and SPOTD algorithms, respectively (See Methods). NCBI RefSeq identifiers are given within brackets. UBZ4: ubiquitin-binding, MLR: primary XPF-binding domain, BTB: homodimerization domain (also contributes to XPF-binding), TBM: TRF2-binding motif, SIM: SUMO-interacting motifs, SAP: MUS81-binding region, CCD: SLX1-binding domain.

(e) YFP-pull downs from HeLa cells expressing WT or mutated YFP-SLX4. ΔBTB: M_{684}VNN-GLPP$_{764}$ was deleted from the BTB domain. BTB5A and SIM: point mutations in the BTB domain and SIM motifs, respectively, as described in[2]. D614G and L618P: cancer-associated mutations (Fig. 1d).

(f) YFP-pull downs from HeLa cells expressing WT or mutated YFP-SLX4. L1022A: TRF2-binding defective mutant.

All immunoblots were performed with antibodies against the indicated proteins.

Uncropped images for panels a, b, d-f and data for graphs in panel b are available as source data.

Fig. 2: Mapping the interaction domains of SLX4 and RTEL1

(a) Schematic of the RTEL1 protein (top) and 3D modelling (ribbon representation) of HD1 and HD2, on which the SLX4 peptide has been docked.

(b) Co-immunoprecipitation of endogenous SLX4 with Flag-tagged full-length RTEL1 or a fragment containing the two harmonins (763-1164) indicated in (**a)**. Immunoblots were performed with antibodies against SLX4 or the Flag peptide. *Flag indicates the band corresponding to Flag-RTEL1 full-length and the Flag-RTEL1$_{763-1164}$ fragment.

(c) Schematic of RTEL1 fragments containing HD1 and/or HD2 (top panel) that were used to assess direct binding to the SLX4$_{577-685}$ (Helix) and SLX4$_{577-1042}$ (Helix+BTB) fragments by Y2H (bottom panel). SLX4-interacting fragments are in red. SD: media complemented with all amino acids except Leu and Trp; X-Gal: ß-galactosidase test; -URA: same as -Leu-Trp with no uracil; 5-FOA: same as -Leu-Trp complemented with 0,2% 5-Fluoroorotic acid; 3-AT: same as –Leu-Trp with no histidine and complemented with 50mM 3-Amino-1,2,4-triazole.

(d) Y2H carried out with WT or mutated SLX4$_{577-1042}$ (Helix+BTB) fragment and the RTEL1$_{885-990}$ fragment (HD1b in **Fig. 2c**). All interaction assays are in duplicate. Media are indicated as in (**c)**.

(e) *E.coli*-produced 6His-tagged HD1b (RTEL1$_{885-990}$) and HD2a (RTEL1$_{1046-1142}$) fragments were used in a Ni^{++}-pull down assay with a WT or a mutated GST-tagged SLX4$_{577-1042}$ (Helix+BTB) fragment. Ni^{++}-agarose beads were resuspended in a volume of Laemmli buffer equivalent to the initial volume of the assay. Identical volumes of Helix+BTB fragments, diluted in Laemmli buffer to the final concentration used in the assay, and of the Ni^{++}-agarose beads resuspended in Laemmli buffer were loaded on the gel.

(f) Schematic of RTEL1 fragments used in **g** and **h** with Hoyeraal-Hreidarsson syndrome (HHS) patient mutations mapped in HD1.

(g,h) Co-immunoprecipitation of endogenous SLX4 with transiently expressed WT or mutated YFP-RTEL1 fragments. Immunoblots were performed with antibodies against the indicated proteins.

Uncropped images for panels b-e,g,h are available as source data.

Fig. 3: SLX4 promotes replication fork progression during S phase through interaction with RTEL1

(a) HeLa Flp-In TREX "Fit0" cells (empty FRT site) were transfected with siRNAs targeting SLX4 (siSLX4^{UTR} and siSLX4^{SP}) or control siRNAs (siLUC). Nascent DNA was labelled with pulses of iododeoxyuridine (IdU) and chlorodeoxyuridine (CldU). Replication fork dynamics were analysed on stretched DNA after immunostaining of IdU, CldU and DNA (red, green and blue, respectively). Distributions of replication track lengths and fork ratios (ratio between the longest tract over the shortest for each individual unbroken fork) are shown in box-plots (median, first and third quartiles) with 5th-95th percentile whiskers (+=mean; dots= outliers; n=number of unbroken signals analysed by Mann-Whitney test, **: p<0.01, ****: p<0.0001). The immunoblot was performed with antibodies against SLX4 and ß-catenin (internal loading control). Arrow: SLX4 band. *: prominent non-specific band. Scale bar = 10 μm.

(b) HeLa "Fit0" and Hela cells stably expressing DOX-inducible WT or mutated Flag-HA-SLX4 as indicated. siSLX4^{UTR} was used to deplete endogenous SLX4. ns: not significant; **: p<0.01; ***: p<0.001; ****: p<0.0001 by Mann-Whitney test. Scale bar = 10 μm.

(c) Nascent DNA strands were pulse-labelled with 5-ethynyl-2-deoxyuridine (EdU). Biotin was conjugated to EdU by click chemistry after cell fixation. *In situ* proximity ligation assay (PLA, green) was performed between SLX4 (anti-HA) and EdU (anti-biotin) before EdU counterstaining (red). Representative fields and zooms on single cells (white squares) are shown. The number of PLA spots per EdU-positive cells is plotted (red bars: median with interquartile range; n>79; Kruskal-Wallis test, ****: p<0.0001). In parallel, single-cell expression of the different Flag-HA-SLX4 constructs was assessed by HA immunostaining (n>99). Parental HeLa "Fit0" cells (-) were used as negative control. Scale bar = 10 μm.

(d) Replication fork dynamics analysed as in **a** in HHS-patient derived SV40-transformed fibroblasts (P7) bearing a homozygous RTEL1^{R957W} mutation in HD1 that abrogates interaction with SLX4 (Fig. 2g,h and Extended data Fig 4). P7 cells were compared to SV40-immortalized fibroblasts expressing WT RTEL1. ****: p<0.0001 by Mann-Whitney test. Scale bar = 10 μm.

Uncropped images of the immunoblots in panel a and data for graphs in panels a-d are available as source data.

Fig. 4: SLX4 promotes replication fork progression independently of its associated SSEs

(a) Schematic of SLX4 showing the F529LW > ALA, E1577L > AA and C1805 > R point mutations introduced to generate the $SLX4^{-SMX}$ mutant that abrogate binding to XPF, MUS81 and SLX1, respectively.

(b) anti-Flag immunoprecipitations were performed on cell lysates from HeLa "Fit0" and HeLa Flp-In TREX cells stably expressing DOX-inducible WT or Flag-HA-$SLX4^{-SMX}$ as indicated. Immunoblots were performed with antibodies against SLX4, XPF, MUS81 and SLX1. The fraction of SLX1, MUS81 and XPF associated with SLX4 was normalized to the total immunoprecipitated SLX4. The relative ratio of SLX1, MUS81 and XPF associated with $SLX4^{-SMX}$ was then normalized to the corresponding $SLX4^{WT}$ ratio.

(c) Replication fork dynamics were assessed as in Fig. 3 in HeLa "Fit0" and HeLa Flp-In TREX cells stably expressing DOX-inducible Flag-HA-$SLX4^{-SMX}$. $siSLX4^{UTR}$ was used to deplete endogenous SLX4. Box-plots show median, first and third quartiles with 5th-95th percentile whiskers (+=mean; dots= outliers; n=number of unbroken signals analysed). ns: not significant; *: $p<0.05$; **: $p<0.01$; ****: $p<0.0001$ by Mann-Whitney test.

Uncropped images of blots for panels b and c and data for co-IP ratios in b and graphs in c are available as source data.

Fig. 5: SLX4 and RTEL1 interaction promotes FANCD2:RNA pol II colocalization and prevents conflicts between replication and transcription

(a) Quantification of FANCD2 foci in unchallenged interphase U2OS "Fit0" cells or expressing WT or mutated Flag-HA-SLX4. The number of foci per cell with the mean ± s.e.m. of the distribution is plotted (n=120 cells). Cells were mock- (siLUC) or SLX4-depleted (siSLX4^{UTR}). Immunoblots at top were performed with anti-SLX4, anti-RTEL1, anti-XPF and anti-GRB2 (loading control).

(b) PLA between FANCD2 and RNA pol II phospho S2 in HeLa "Fit0" cells mock- or SLX4-depleted. Reactions with single primary antibodies (Ab) were used as negative controls. Box-plots show number of PLA spots per nucleus (n>180; median, first and third quartiles, 5-95th percentile whiskers, +: mean). Immunoblot at right was performed with anti-SLX4 or anti-ß-catenin (loading control). The arrow indicates the SLX4 band.

(c) As in **b**, in U2OS cells expressing Flag-HA-SLX4 (n>180). Endogenous SLX4 was depleted with siSLX4^{UTR}.

(d) PLA between SLX4 (HA) and RNA pol II phospho S2 in U2OS cells expressing Flag-HA-SLX4^{WT} (left panel, n>139, median with interquartile range). Parental U2OS "Fit0" cells (-) were used as a negative control. Right panel shows single-cell expression of the construct (HA staining, n>124).

(e) PLA between endogenous RTEL1 and RNA pol II phospho S2 in HeLa "Fit0" cells (n>153). PLA negative controls as in **b**.

(f) PLA between endogenous PCNA and RNA pol II phospho S2 was performed in mock-depleted (siLUC), SLX4-depleted (siSLX4^{UTR}, siSLX4^{sp}) or RTEL1-depleted (siRTEL1) HeLa "Fit0" cells (n>175). PLA negative controls as in **b**.

Kruskal-Wallis (**a**, **b**, **c**, **e**, **f**) and Mann-Whitney (**d**) tests (ns: not significant, *: $p<0.05$, **: $p<0.01$, ***: $p<0.001$, ****: $p<0.0001$). Scale bar of representative fields and cells = 10 μm in all panels.

Uncropped images of the immunoblots in panels a,b and data for graphs in panels a-f are available as source data.

Fig. 6: Transcription inhibition rescues replication defects caused by loss of SLX4-RTEL1 complex formation

(a) HeLa "Fit0" cells were depleted for SLX4 or RTEL1 and 50 μM cordycepin was added to culture medium 3 h before and during the IdU and CldU pulses to inhibit transcription elongation. Replication fork dynamics were analysed as in **Fig. 3a**. The distribution of the fork ratio is shown in box-plots (median, first and third quartiles with 5th-95th percentile whiskers; +=mean; dots= outliers; n=number of unbroken signals analysed; ns: not significant, **: $p<0.01$, ****: $p<0.0001$ by Mann-Whitney test). See also Extended Data Fig. 8a for the distributions of replication track lengths and western blot showing depletion efficiency.

(b) As in **a** in HeLa Flp-In TREX cells stably expressing DOX-inducible WT, D614G or L618P Flag-HA-SLX4 depleted for endogenous SLX4. The immunoblot was performed with antibodies against SLX4 and ß-catenin used as internal loading control.

(c) As in **a** in $RTEL1^{WT}$ and $RTEL1^{R957W}$ SV-40 immortalized human fibroblasts.

Uncropped images of the immunoblots in panel b and data for graphs in panels a-c are available as source data.

METHODS

DNA construction and mutagenesis

DNA constructions and cloning were performed using Gateway Technology (Invitrogen) as per manufacturer's instruction. A list of primers used in this study is available upon request. The BTB and SIM mutants of SLX4 were generated as previously described[2]:

$SLX4^{BTB*}$ ($H_{706}KFVL_{710}$ → AAAAA)

$SLX4^{SIM*}$ (SIM1: $V_{1151}ILLL_{1155}$ →AAAAA; SIM2: $I_{1194}IDV$ → AADV; SIM3: $V_{1392}VEV$ →AAEV)

In addition, a deletion of the BTB domain was generated and used in the present study:

$SLX4^{\Delta BTB}$ (deletion $M_{684}VNN$-$GLPP_{764}$)

$SLX4^{-SMX}$ ($F_{529}LW$ →ALA, $E_{1577}L$ →AA, C_{1805} →R)

Antibodies

Rabbit anti-SLX4 (A302-270A), rabbit anti-XPF (A301-315A-T), rabbit anti-biotin (A150-109A) and rabbit anti-TRF2 (A300-796A) antibodies were purchased from Bethyl. Rabbit anti-RTEL1 antibody was produced by the laboratory of Arturo Londoño-Vallejo's[64]. Mouse anti-MUS81 [MTA30 2G10/3] (ab14387), mouse anti-GAPDH (ab9484), rabbit anti-FANCD2 (ab2187) and rabbit anti-RNA polymerase II (ab5095 [phospho S2]) antibodies were purchased from Abcam. Mouse anti-RNA polymerase II (clone H5 MMS-129R [phospho S2]), mouse anti-HA [16B12] (901513) antibodies were purchased from BioLegend. Mouse anti-XPF [clone 219] (XPF Ab-1) antibody was from Thermo scientific. Mouse anti-ß-catenin (clone 14, 610153) and mouse anti-GRB2 (610111) antibodies were from BD Biosciences. Mouse anti-ß-actin antibody (AC-15, A5441) was purchased from Sigma. Mouse anti-laminA/C antibody was purchased from Santa Cruz (sc-7292). Mouse anti-BrdU antibody (clone B44, 347580) was from Becton Dickinson. Rat anti-BrdU antibody (clone BU1/75, AbC117-7513) was purchased from Abcys. Mouse anti-ssDNA antibody (clone 16-19, MAB3034) was from Millipore. Mouse anti-biotin antibody (200-002-211) was purchased from Jackson Immunoresearch.

Duolink® In Situ PLA® Probe anti-Rabbit PLUS (DUO92002) anti-Mouse MINUS (DUO92004) were from Sigma.

Goat anti-rabbit IgG/HRP (2019-08) and goat anti-mouse IgG/HRP (2019-05) antibodies were purchased from Dako. Alexa Fluor 488 conjugated donkey anti-mouse (A-21202), goat anti-mouse (A-11001), goat anti-rat (A-11006) and Alexa Fluor 594 conjugated donkey anti-rabbit (A-21207), goat anti-mouse (A-11032 and A-11020), goat anti-rabbit (A-11072), rabbit anti-mouse (A-21062), goat anti-rabbit (A-11046) antibodies were from Molecular probes.

Immunoblotting

SDS-PAGE and immunoblotting were done with Novex® NuPAGE® SDS-PAGE Gel System and XCell II™ blot module (Invitrogen), respectively. Hybond-C Extra (RPN203e) was purchased from GE healthcare. Western lightning plus ECL (NEL105001eA) was from PerkinElmer, Hyperfilm ECL (28-9068-35) was purchased from GE healthcare. Chemidoc MP imaging system (Biorad), ImageQuant LAS 4000 system (GE Healthcare) or Amersham Imager 600 (GE health care) were also used for detection.

Cell lines, cell culture and transfection

HeLa cells (ATCC) were cultured in DMEM with 10% FBS and Pen/Strept (Gibco). HeLa Flp-In TRex and U2OS Flp-In TRex cells (Fit0: parental cells with no cDNA integrated at the FRT site) (kindly provided by Stephen Taylor and Palm Silver, respectively) were maintained in DMEM containing 10% FBS and Pen/Strept with 2 µg/mL Blasticidine (Invivogen) and 100 µg/mL Zeocin (Invitrogen) to maintain the genomic FRT site. For generating stable cell lines expressing YFP- or Flag-HA- tagged SLX4 in a doxycycline-inducible manner, pDEST-YFP-SLX4 or pDEST-Flag-HA-SLX4 were co-transfected with pOG44 (encoding the Flp recombinase) with 1:9 ratio, respectively, using JetPEI (Polyplus transfection) as per manufacturer's instruction. Recombinant clones were selected with the medium described above with 100 µg/mL Hygromycin B (Invitrogen) instead of Zeocin. Selected clones were pooled to generate a population in order to minimize clonal heterogeneity. Fibroblasts from a severe combined immunodeficient patient with genetic defect in the lymphoid specific RAG1 gene that is not expressed in fibroblasts (WT RTEL1 control in Extended data Fig. 6c) and from an RTEL1-deficient patient P7[31] were obtained from skin biopsies. Informed and written consent was obtained from donors and patients. The study and protocols comply with the 1975 Declaration of Helsinki as well as with the local legislation and ethical guidelines from the Comité de Protection des Personnes de l'Ile de France II and the French advisory committee on data processing in medical research. Fibroblasts were transformed by the large T antigen from SV40T as previously described[65]. Fibroblasts were cultured in RPMI with 15% FBS, Pen/Strept and 25 mM Hepes (Gibco) under 3% O_2. All cell lines were checked for mycoplasma contamination.

Immunoprecipitation

In YFP-pull downs, the SLX4 complex was purified from HeLa Fit0 cells transfected with pDEST-YFP-SLX4 or HeLa Flp-In TREX cells expressing YFP-SLX4 under 10 ng/mL doxycycline, as previously described[2]. Briefly, cells were harvested by Trypsin/EDTA, washed with PBS then lysed with NETN buffer (50 mM Tris-HCl [pH 8.0], 150 mM NaCl, 1 mM EDTA, 1% NP-40, 1 mM DTT, 0.25 mM PMSF) containing proteasome inhibitor cocktail (Complete EDTA-free [Roche]) for 30 min at 4˚C. After centrifugation (15000 rpm, 10 min at 4˚C),

supernatants were incubated with GFP nanobody (kindly provided by Mauro Modesty) for 2 hrs at 4˚C. The beads were washed 3 times with NETN buffer, twice with TBS, and 5 times with 50 mM Tris-HCl [pH 8.0] before samples were eluted with NuPAGE LDS sample buffer (Invitrogen) for 5 min at 95˚C. For Fig. 1a (lane 3), NETN buffer including 850 mM NaCl was added to the supernatant before immunoprecipitation to adjust the final concentration of NaCl to 500 mM. After the incubation, beads were washed with NETN including 500 mM NaCl for 3 times before TBS wash. For Fig. 1a (lane 4 and 5), beads were incubated with either 500 U/mL Benzonase (Sigma) in presence of 2 mM $MgCl_2$ or 50 µg/mL EtBr for 16 hrs after TBS wash. Beads were washed 5 times with 50 mM Tris-HCl [pH 8.0] buffer then samples were eluted with NuPAGE LDS sample buffer. For anti-Flag immunoprecipitation samples were processed as described above using FLAG M2 Agarose beads (Sigma-Aldrich) instead of a GFP-nanobody.

Co-immunoprecipitation of endogenous SLX4 and RTEL1

10^7 HeLa (Fit0) cells were lysed in NETN buffer (50 mM Tris-HCl [pH=8.0], 150 mM NaCl, 1 mM EDTA, 0.5% NP-40 supplemented with anti-proteases cocktail (Roche)) at 4°C before sonication and centrifugation. Half of the clarified lysate were incubated either with 2µg of IgG rabbit (Cell Signaling #2729S)) or 2µg of anti-SLX4 (1µg of A302-270A + 1µg A302-269A from Bethyl laboratories) and 15µL dynabeads-protein G (invitrogen) overnight at 4°C. Beads were washed 4 times in NETN buffer before elution in loading buffer. To probe for RTEL1 and SLX4 in WB and avoid the signal of the IgG used for immunoprecipitation, specific secondary antibodies were used (Veriblot, Abcam).

Cell cycle synchronization

HeLa Flp-In TREX cells expressing Flag-HA-SLX4 were synchronized by double thymidine block. $2x10^6$ cells were seeded the day before treatment then incubated with 10% FBS/DMEM containing 2 mM Thymidine (Sigma) and doxycycline (10 ng/mL) for 18 hrs. After PBS wash, cells were incubated in the medium without Thymidine for 9 hrs then incubated in the medium containing 2 mM of Thymidine for 16 hrs. The cells synchronized at G1/S phase were released from Thymidine block and collected at several time points after release (described in the Fig.). Cell cycle stages of samples were analyzed with a Muse™ cell analyser (Millipore) as per manufacturer's instructions.

Yeast Two Hybrid

Yeast Two-Hybrid assay was performed using ProQuest Two-Hybrid systems as per manufacturer's instruction. Briefly, various Human SLX4 and RTEL1 cDNA fragments indicated in Fig. 2c,d and Extended data Fig. 4 were inserted in yeast two-hybrid vectors pDEST22 and pDEST32, respectively. Yeast two-hybrid vectors were transformed into the yeast strain

MaV203. Cells were cultured on plates with the selective media as indicated in Fig. 2c,d and Extended data Fig. 4.

Protein Expression and Purification and *in vitro* binding assay

The 6His-tagged RTEL1 HD1a, HD1b and H2a fragments and the GST-SLX4 (Helix-BTB) WT and D614G mutant fragments were expressed in *E.coli* (Rosetta) induced with 0.1 mM IPTG at 16°C overnight. Bacterial pellets were frozen in PBS. The next day, an equivalent volume of 2x lysis buffer (100 mM Tris [pH=8], 20% [v/v] glycerol, 2% [v/v] Triton X-100, 1 M NaCl, 1 mg/ml lysozyme (Sigma)) was added. A protease inhibitor cocktail (Complete EDTA-free, Roche) and PMSF were added to the thawed lysates just before sonication and clarification.

Ni^{++}-agarose was charged with the 6His-tagged RTEL1 HD fragments after incubation with the supernatant for 3 hrs at 4°C. The Ni++-agarose resin was washed 5 times in wash buffer (50 mM Tris.Cl pH=8, 1 M NaCl, 0.01% [v/v] Triton X-100) and stored at 4°C in binding buffer (150mM NaCl, Tris.Cl pH=8, 0,01% [v/v] Triton X100, 10% [v/v] glycerol). The GST-SLX4 (Helix-BTB) WT and D614G mutant fragments were purified on Glutathione agarose (Molecular probes) following standard procedures

For *in vitro* binding assays the GST-SLX4 (Helix-BTB) fragments were incubated with Ni^{++}-agarose charged with the 6His-tagged RTEL1 HD fragments for 2 hours at 22°C. The flow through (Ft) was recovered after centrifugation. The pelleted Ni^{++}-agarose was subsequently was washed 10 times with 10 bead volume of binding buffer before it was resuspended in a volume of Laemmli buffer equivalent to the total volume of the *in vitro* binding assay.

Proteins were analyzed by SDS-PAGE and detected following transfer to a nitrocellulose membrane (Amersham) with anti-6His or anti-GST antibodies.

siRNA transfection and Complementation assays

The following siRNA sequences were used in this work.

siLUC (CGUACGCGGAAUACUUCGAdTdT)

$siSLX4^{UTR}$ targeting the 5'UTR and 3'UTR of SLX4 consists of a mix of two siRNAs:

SLX4 UTR87 (GCACCAGGUUCAUAUGUAUdTdT)

SLX4 UTR7062 (GCACAAGGGCCCAGAACAAdTdT)

In addition, siRNAs for SLX4 (M-014895-01-0005) ($siSLX4^{SP}$) and RTEL1 (M-013379-00-0005) ($siRTEL1^{SP}$) were purchased from Dharmacon.

Fit0 cells or stable cell lines described in Cell lines section were seeded the day before transfection ($1.5x10^5$ cells/6-well). The transfection was performed in 10%FBS/DMEM containing doxycycline to induce Flag-HA-SLX4 protein expression. siRNAs were transfected at 10 or 20 nM of final siRNA concentrations using INTERFERin (Polyplus transfection) as per manufacturer's instructions. The transfection was repeated 24 hrs later then cells were

reseeded 6 hrs after the 2nd siRNA transfection. Cells were then incubated in 10%FBS/DMEM containing doxycycline for 1 or 2 days in order to achieve optimal knockdown efficiency and to maintain Flag-HA-SLX4 expression. Cell biological and biochemical analysis were performed as described below.

Colony survival assay

siRNA-treated HeLa Flp-In TREX cells expressing Flag-HA-SLX4 were reseeded at 900 cells/60 mm Petri dish 6 hrs after the 2nd siRNA transfection. 20 hrs later, cells were treated with the indicated concentrations of mitomycin C (MMC) in presence of doxycycline (1 ng/mL) for 24 hrs. Cells were then subsequently washed with PBS and cultured with 10% FBS/DMEM including 1 ng/ml of doxycycline. Colonies were fixed with fix solution (50% EtOH, 7% Acetic acid) including 0.5 mg/mL Brilliant blue R 250 (Sigma) 8 days after MMC treatment and counted.

DNA fiber analysis

Cells were pulse labelled with 25 μM IdU (Sigma) for 20 min, washed with pre-heated medium and PBS, then pulse labeled with 50 μM CldU (Sigma) for 20 min. In Fig. 6 and Extended data Fig. 8a, cells were pre-treated for 3 h with 50 μM cordycepin (Sigma) and cordycepin was maintained during the labelling procedure. In Extended data Fig. 8b, cells were treated for 3 h with 1 μM triptolide (Sigma) and triptolide was maintained during the labelling procedure. Cells were harvested by trypsinization and resuspended in ice-cold PBS at 500,000 cells per ml. 2 μL of the cell suspension (1,000 cells) were spotted on microscope glass slides and lyzed in 7 μL of spreading buffer (200 mM Tris-HCl [pH 7.5], 50 mM EDTA [pH8.0], 10% SDS). Slides were tilted to 15˚ in order to spread the DNA molecules. After fixation with a mixture of methanol and acetic acid (3:1), air-dried slides were incubated twice in H_2O for 5 min followed by denaturation in 2.5 M HCl for 1 hr. Slides were washed in PBS and blocked for 1 h in blocking buffer (1% BSA, 0.1% Tween20 in PBS). IdU, CldU and total DNA were immunodetected with the following procedure: (1) mouse anti-BrdU (clone B44 347580, Becton Dickinson, 1/20, IdU) + rat anti-BrdU (clone BU1/75 AbC117-7513, Abcys, 1/100, CldU) for 1 h at room temperature, (2) goat anti-mouse AF594 (A11032) + goat anti-rat AF488 (A11006) for 30 min at 37°C, (3) mouse anti-single stranded DNA (clone 16-19 MAB3034, Ozyme, 1/100) for 45 min at 37°C, (4) rabbit anti-mouse AF350 (A21062) for 20 min at 37°C and (5) goat anti-rabbit AF350 (A11046) for 20 min at 37°C. All AlexaFluor-coupled antibodies were from Molecular probes and used at 1/100 dilution. All antibodies were diluted in blocking buffer. Samples were mounted in fluorescent mounting medium (DAKO). Images were acquired on an Axio Imager Z1 microscope using the Axio Vision software (Zeiss). Images were analyzed with the Axio Vision software. Broken replication tracks, established by total DNA counterstaining, were excluded from the analysis.

For each intact individual fork (i.e. one IdU tract flanked by a CldU track), the fork ratio was calculated as the ratio between max(IdU,CldU) and min(IdU,CldU).

Immunofluorescence

siRNA-treated HeLa Flp-In TREX or U2OS Flp-In TREX cells expressing Flag-HA-SLX4 or YFP-SLX4 were cultured on coverslips. Cells were washed with CSK buffer (100 mM NaCl, 300 mM sucrose, 10 mM PIPES [pH 7.0], 3 mM $MgCl_2$) and pre-extracted in CSK buffer containing 0.5% TritonX-100 for 3 min at 4˚C then fixed in 4% paraformaldehyde/PBS. For Extended data Fig. 1b, HeLa Flp-In TREX cells expressing YFP-SLX4 were washed with PBS and fixed in 4% paraformaldehyde/PBS then permeabilized in 0.5% TritonX-100/PBS for 15 min. After PBS wash, cells were incubated in blocking buffer (3% BSA/PBS) for 30 min then immunostained with primary antibodies in blocking buffer for 2 hrs at room temperature or overnight at 4˚C. Cells were washed three times with blocking buffer and stained with secondary antibodies in blocking buffer for 2 hrs at room temperature. After three times of PBS wash, coverslips were mounted in fluorescent mounting medium supplemented with DAPI (Vector Laboratory or Dako). Images were acquired with LSM-880 microscope using Zen software (Zeiss) (Fig. 4a) or with Axio Imager Z1 and Z2 microscope using Axio Vision software (Zeiss) (Extended data Fig. 1c). Images were analyzed with ImageJ software.

***In situ* Proximity ligation assay (PLA)**

For PLA, cells were seeded on fibronectin-coated glass coverslips. PLA between SLX4, RTEL1 or FANCD2 and RNA polymerase II were performed as described previously[34]. Cells were fixed with 4% paraformaldehyde/PBS and permeabilized in 0.5% TritonX-100/PBS for 5 min. PLA was performed with the Duolink PLA *In situ* Green kit (Sigma) according to manufacturer's instructions. The following couples of primary antibodies were used: mouse anti-HA [16B12] (to detected SLX4, 1/1000) + rabbit anti-RNA polymerase II ab5095 (1/900); mouse anti-RNA polymerase II MMS-129R (1/600) + rabbit anti-FANCD2 ab2187 (1/1000) or rabbit anti-RTEL1 (1/500). When indicated, HA counterstaining was performed by incubating the coverslips with goat anti-mouse AF594 after the PLA procedure.

PLA between SLX4 and nascent DNA was performed as described previously[66], with minor modifications. Briefly, cells were pulse labeled with 30 μM EdU for 7 min, pre-extracted with CSK100 buffer (100 mM NaCl, 300 mM sucrose, 10 mM PIPES [pH 6.8], 3 mM $MgCl_2$, 1 mM EGTA, 0.5% TritonX-100, protease inhibitors) for 5 min at 4 ˚C and fixed. Biotin-azide (Molecular Probes) was conjugated to EdU by click chemistry. PLA was performed using mouse anti-HA [16B12] (1/1000) and rabbit anti-biotin (A150-109A, Bethyl, 1/3000) antibodies or mouse anti-biotin (1/3000) and rabbit anti-RTEL1 (1/500) antibodies. PLA was followed by EdU counterstaining.

Bioinformatic and structural analyses

Homolog Sequences of RTEL1 and SLX4 were retrieved using PSI-BLAST searches[67] against the RefSeq database. Multiple sequence alignments were calculated using MAFFT (e-insi mode)[68] and represented using Jalview[69]. Secondary structures (H for helix, E for extended) and disorder status (d) were predicted by PSIPRED[70] and SPOTD[71] algorithms, respectively. 3d models of the HD1 and HD2 harmonin domains of human RTEL1 in complex with the helix of human SLX4 were generated by template-based docking using the alignments calculated by hhpred[72] and the RosettaCM[73] protocol for comparative modeling. As a structural template the structure (PDB code:4yl6) of the complex between the harmonin domain of CCM2 and the MEKK3 helix[74] was used as it was the best hhpred hit obtained from an X-ray structure (hhpred proba of 98.2% and 97.8% for HD1 and HD2, respectively). HD1 and HD2 share 21% and 17% sequence identity with CCM2, respectively, while SLX4 shares significant similarities with MEKK3 sequence, which were used to align both ligands sequences.

Next generation sequencing of clinical samples

Targeted NGS was applied to a custom-made panel of 494 “cancer-associated” genes selected for their involvement in cancers (CCP-V8 panel). The DNA libraries of all coding exons and intron-exon boundaries of all genes using the HaloPlex Target Enrichment System (Agilent, Santa Clara, CA, USA) were done as described[75]. Sequencing was done using the 2×150-bp paired-end technology on the Illumina Nextseq500 platform according to the manufacturer's instructions (Illumina, San Diego, CA, USA). To identify somatic mutations only, germline DNAs from normal counterpart samples (blood lymphocytes of corresponding patients) were similarly sequenced. Samples were biopsied metastases from patients enrolled in the prospective PERMED-01 trial (NCT02342158)[76]. Samples were sequenced at an average depth greater than 700x for the targeted regions. PERMED 1069 was a liver metastasis of gastric adenocarcinoma; the SLX4 NM_032444 exon8 c.T1853c p.L618P variant had an allelic frequency of 2.30% (the ratio of malignant cells was 30%). PERMED 1115 was a lung metastasis of chondroblastic osteosarcoma; the SLX4 NM_032444 exon8 c.A1841G p.D614G variant had an allelic frequency of 6.80% (the ratio of malignant cells was 90%).

Mass spectroscopy and data analysis methods are presented as a Supplementary Note.

Statistics

GraphPad Prism 6 software was used for statistics. Statistical comparisons of replication track length and fork ratio distributions were assessed with the non-parametric two-tailed Mann–

Whitney test. IF and PLA experiments were tested with the non-parametric two-tailed Kruskal-Wallis followed by Dunn's multiple comparisons. Complete results of statistics tests are shown in the Source Data files.

DATA AVAILABILITY

The data supporting the findings of this study are available with the online article. The mass spectrometry proteomics data have been deposited to the ProteomeXchange Consortium via the PRIDE [1] partner repository with the datasets identifiers PXD012426 and PXD012425. Next Generation sequence data (PERMED 1069 = isolate P1, PERMED 1115 = isolate P2) were deposited in the Sequence Read Archive (SRA) under the BioProject PRJNA611917 and can be retrieved at https://www.ncbi.nlm.nih.gov/Traces/study/?acc=PRJNA611917

Reporting summary. Further information on experimental design is available in the Nature Research Reporting Summary linked to this paper.

METHODS-ONLY REFERENCES

64. Le Guen, T. *et al.* Human RTEL1 deficiency causes Hoyeraal-Hreidarsson syndrome with short telomeres and genome instability. *Hum Mol Genet* **22,** 3239–3249 (2013).
65. Buck, D. *et al.* Cernunnos, a novel nonhomologous end-joining factor, is mutated in human immunodeficiency with microcephaly. *Cell* **124,** 287–299 (2006).
66. Despras, E. *et al.* Rad18-dependent SUMOylation of human specialized DNA polymerase eta is required to prevent under-replicated DNA. *Nat Commun* **7,** 13326 (2016).
67. Altschul, S. F. *et al.* Gapped BLAST and PSI-BLAST: a new generation of protein database search programs. *Nucleic Acids Res* **25,** 3389–3402 (1997).
68. Katoh, K. & Standley, D. M. MAFFT multiple sequence alignment software version 7: improvements in performance and usability. *Mol. Biol. Evol.* **30,** 772–780 (2013).
69. Waterhouse, A. M., Procter, J. B., Martin, D. M. A., Clamp, M. & Barton, G. J. Jalview Version 2--a multiple sequence alignment editor and analysis workbench. *Bioinformatics* **25,** 1189–1191 (2009).
70. Jones, D. T. Protein secondary structure prediction based on position-specific scoring matrices. *J Mol Biol* **292,** 195–202 (1999).
71. Hanson, J., Yang, Y., Paliwal, K. & Zhou, Y. Improving protein disorder prediction by deep bidirectional long short-term memory recurrent neural networks. *Bioinformatics* **33,** 685–692 (2017).
72. Zimmermann, L. *et al.* A Completely Reimplemented MPI Bioinformatics Toolkit with a New HHpred Server at its Core. *J Mol Biol* **430,** 2237–2243 (2018).
73. Song, Y. *et al.* High-resolution comparative modeling with RosettaCM. *Structure* **21,** 1735–1742 (2013).
74. Wang, X. *et al.* Structural Insights into the Molecular Recognition between Cerebral Cavernous Malformation 2 and Mitogen-Activated Protein Kinase Kinase Kinase 3. *Structure* **23,** 1087–1096 (2015).
75. Collette, Y. *et al.* Drug response profiling can predict response to ponatinib in a patient with t(1;9)(q24;q34)-associated B-cell acute lymphoblastic leukemia. *Blood Cancer J* **5,** e292 (2015).
76. Chanez, B. *et al.* De novo metastatic small cell carcinoma of the prostate with BRCA2 mutation: report of a successful precision medicine management with PARP inhibitors. JCO Precision Oncology, 2:1-8. doi.org/10.1200/PO.18.00083 (2018)

1039

Figure 1

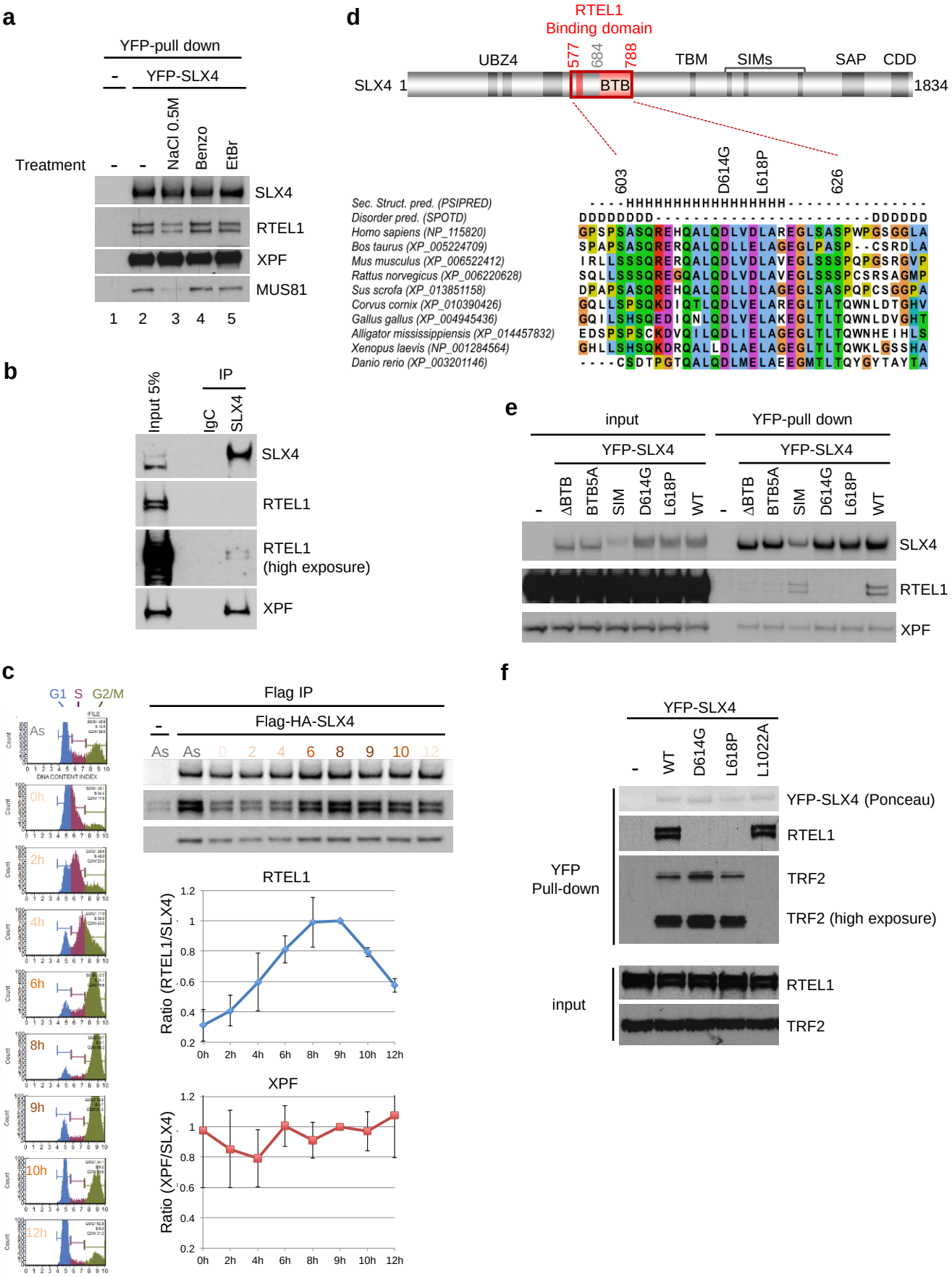
a
YFP-pull down
-
YFP-SLX4
Treatment
-
-
NaCl 0.5M
Benzo
EtBr
SLX4
RTEL1
XPF
MUS81
1 2 3 4 5
b
Input 5%
IP
IgC
SLX4
SLX4
RTEL1
RTEL1
(high exposure)
XPF
c
G1
S
G2/M
As
0h
2h
4h
6h
8h
9h
10h
12h
DNA CONTENT INDEX
Flag IP
-
Flag-HA-SLX4
As As 0 2 4 6 8 9 10 12
RTEL1
Ratio (RTEL1/SLX4)
XPF
Ratio (XPF/SLX4)
0h 2h 4h 6h 8h 9h 10h 12h
d
RTEL1
Binding domain
UBZ4
577
684
788
TBM
SIMs
SAP
CDD
SLX4 1
BTB
1834
603
D614G
L618P
626
Sec. Struct. pred. (PSIPRED)
Disorder pred. (SPOTD)
Homo sapiens (NP_115820)
Bos taurus (XP_005224709)
Mus musculus (XP_006522412)
Rattus norvegicus (XP_006220628)
Sus scrofa (XP_013851158)
Corvus cornix (XP_010390426)
Gallus gallus (XP_004945436)
Alligator mississippiensis (XP_014457832)
Xenopus laevis (NP_001284564)
Danio rerio (XP_003201146)
e
input
YFP-pull down
YFP-SLX4
YFP-SLX4
-
ΔBTB
BTB5A
SIM
D614G
L618P
WT
-
ΔBTB
BTB5A
SIM
D614G
L618P
WT
SLX4
RTEL1
XPF
f
YFP-SLX4
-
WT
D614G
L618P
L1022A
YFP-SLX4 (Ponceau)
RTEL1
TRF2
TRF2 (high exposure)
YFP
Pull-down
input
RTEL1
TRF2

Figure 2

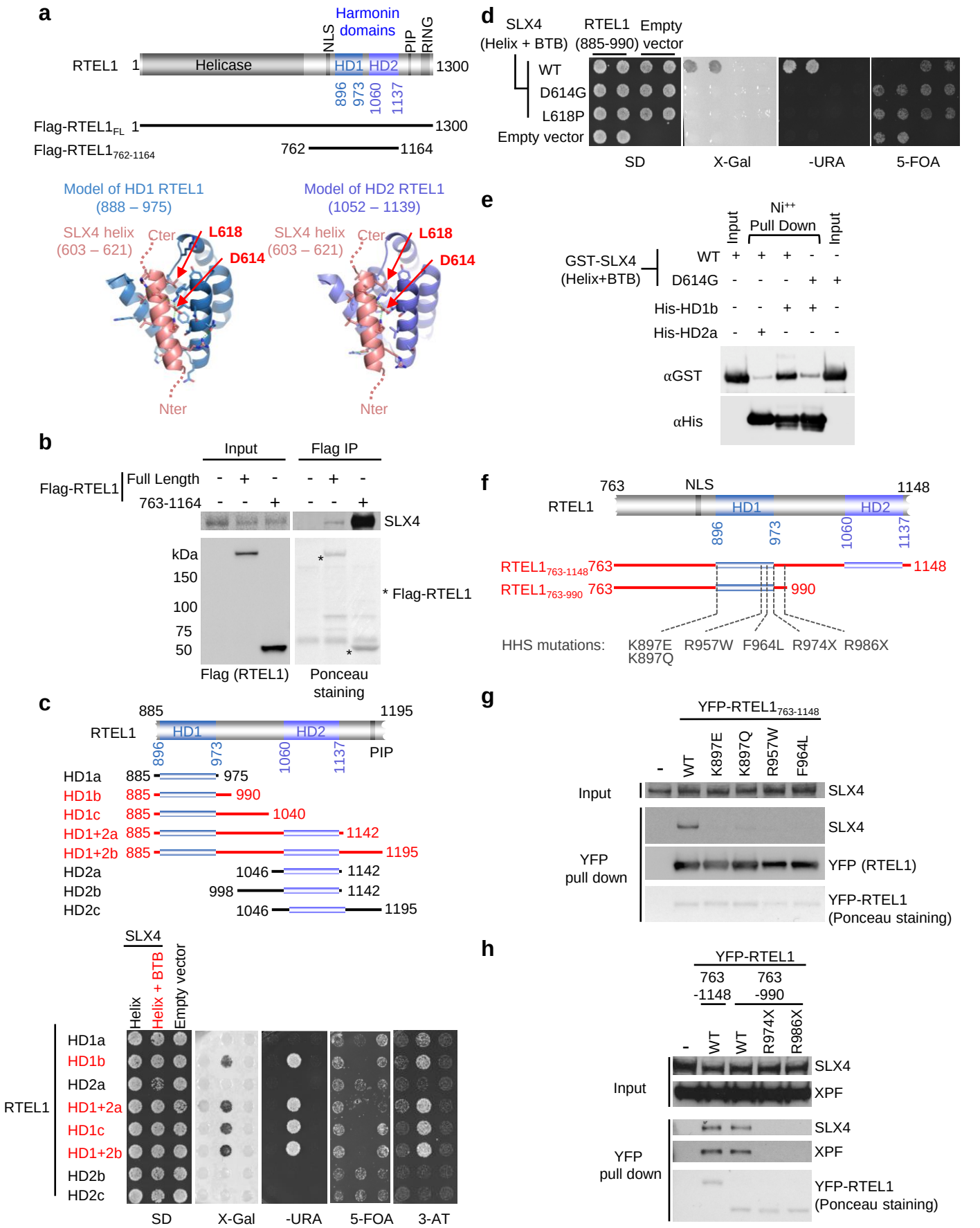
a
Harmonin domains
NLS
PIP
RING
RTELI 1
Helicase
HD1
HD2
1300
896
973
1060
1137
Flag-RTEL1FL 1
1300
Flag-RTEL1762-1164
762
1164
Model of HD1 RTEL1 (888 – 975)
Model of HD2 RTEL1 (1052 – 1139)
SLX4 helix (603 – 621)
Cter
L618
D614
Nter
b
Input
Flag IP
Flag-RTEL1
Full Length
763-1164
SLX4
kDa
150
100
75
50
* Flag-RTEL1
Flag (RTEL1)
Ponceau staining
c
885
1195
RTEL1
HD1
HD2
PIP
HD1a 885 975
HD1b 885 990
HD1c 885 1040
HD1+2a 885 1142
HD1+2b 885 1195
HD2a 1046 1142
HD2b 998 1142
HD2c 1046 1195
SLX4
Helix
Helix + BTB
Empty vector
RTEL1
HD1a
HD1b
HD2a
HD1+2a
HD1c
HD1+2b
HD2b
HD2c
SD
X-Gal
-URA
5-FOA
3-AT
d
SLX4 (Helix + BTB)
RTEL1 (885-990)
Empty vector
WT
D614G
L618P
Empty vector
SD
X-Gal
-URA
5-FOA
e
Ni++ Pull Down
Input
Input
GST-SLX4 (Helix+BTB)
WT
D614G
His-HD1b
His-HD2a
αGST
αHis
f
763
NLS
1148
RTEL1
HD1
HD2
896
973
1060
1137
RTEL1763-1148 763 1148
RTEL1763-990 763 990
HHS mutations:
K897E
K897Q
R957W
F964L
R974X
R986X
g
YFP-RTEL1763-1148
-
WT
K897E
K897Q
R957W
F964L
Input
SLX4
YFP pull down
SLX4
YFP (RTEL1)
YFP-RTEL1 (Ponceau staining)
h
YFP-RTEL1
763 -1148
763 -990
-
WT
WT
R974X
R986X
Input
SLX4
XPF
YFP pull down
SLX4
XPF
YFP-RTEL1 (Ponceau staining)

Figure 3

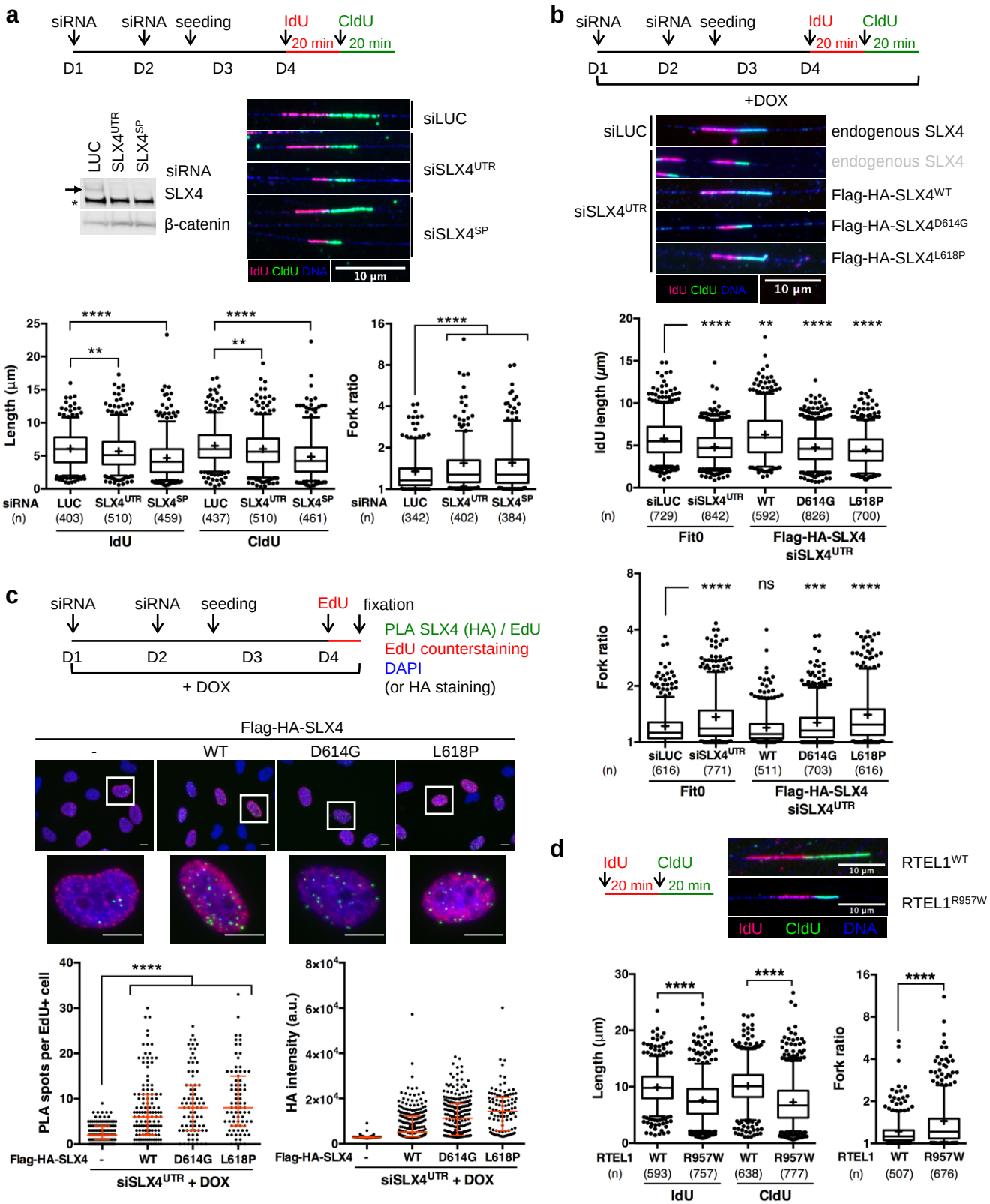
a
siRNA
siRNA
seeding
IdU
20 min
CldU
20 min
D1
D2
D3
D4
LUC
SLX4UTR
SLX4SP
siRNA
SLX4
β-catenin
siLUC
siSLX4UTR
siSLX4SP
IdU CldU DNA
10 µm
Length (µm)
siRNA
LUC
SLX4UTR
SLX4SP
(n)
(403)
(510)
(459)
(437)
(510)
(461)
IdU
CldU
Fork ratio
(342)
(402)
(384)
b
+DOX
endogenous SLX4
Flag-HA-SLX4WT
Flag-HA-SLX4D614G
Flag-HA-SLX4L618P
IdU length (µm)
siLUC
siSLX4UTR
WT
D614G
L618P
(729)
(842)
(592)
(826)
(700)
Fit0
Flag-HA-SLX4
siSLX4UTR
(616)
(771)
(511)
(703)
(616)
ns
c
EdU
fixation
PLA SLX4 (HA) / EdU
EdU counterstaining
DAPI
(or HA staining)
+ DOX
Flag-HA-SLX4
-
WT
D614G
L618P
PLA spots per EdU+ cell
HA intensity (a.u.)
siSLX4UTR + DOX
d
RTEL1WT
RTEL1R957W
RTEL1
R957W
(593)
(757)
(638)
(777)
(507)
(676)

Figure 4

a

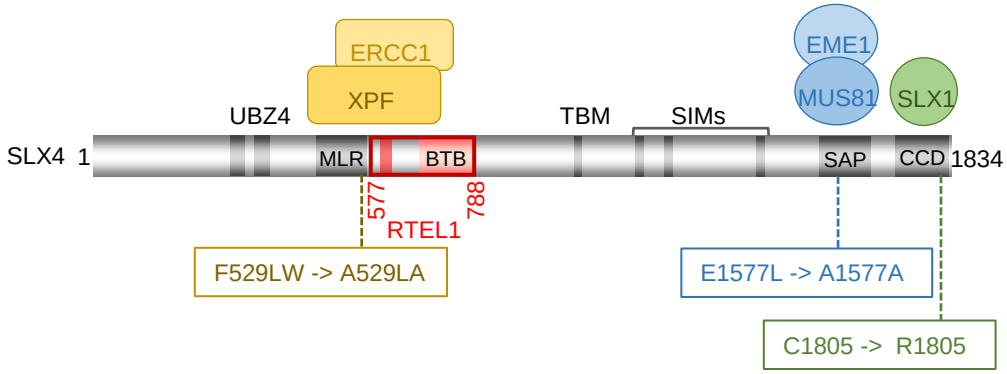
ERCC1
XPF
EME1
MUS81
SLX1
UBZ4
TBM
SIMs
SLX4 1
MLR
BTB
SAP
CCD
1834
577
788
RTEL1
F529LW -> A529LA
E1577L -> A1577A
C1805 -> R1805

b

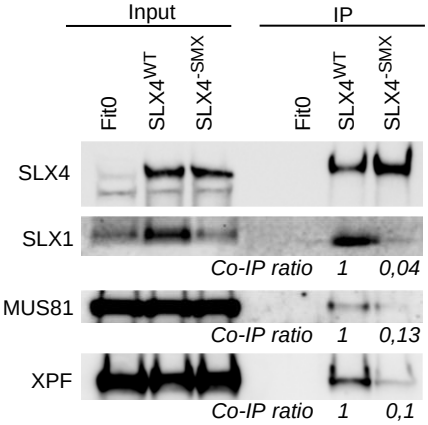
Input
IP
Fit0
SLX4WT
SLX4-SMX
Fit0
SLX4WT
SLX4-SMX
SLX4
SLX1
Co-IP ratio 1 0,04
MUS81
Co-IP ratio 1 0,13
XPF
Co-IP ratio 1 0,1

c

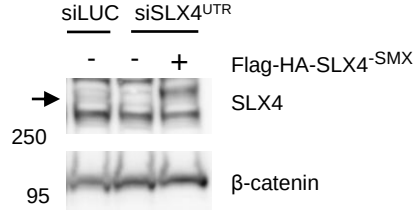
siLUC
siSLX4UTR
- - +
Flag-HA-SLX4-SMX
SLX4
250
95
β-catenin

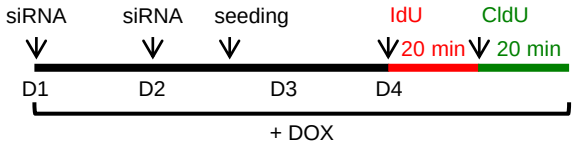
siRNA
siRNA
seeding
IdU
CldU
20 min
20 min
D1
D2
D3
D4
+ DOX

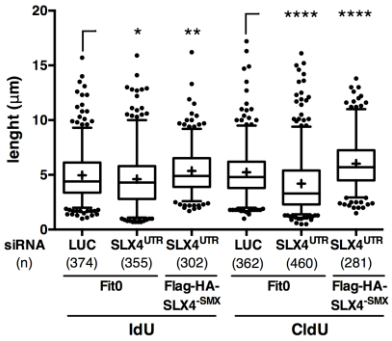
lenght (µm)
20
15
10
5
0
*
**
****
****
siRNA
(n)
LUC
(374)
SLX4UTR
(355)
SLX4UTR
(302)
LUC
(362)
SLX4UTR
(460)
SLX4UTR
(281)
Fit0
Flag-HA-SLX4-SMX
Fit0
Flag-HA-SLX4-SMX
IdU
CldU

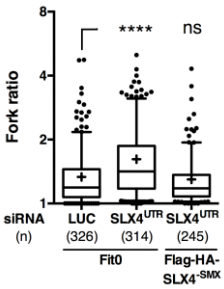
Fork ratio
8
4
2
1
****
ns
siRNA
(n)
LUC
(326)
SLX4UTR
(314)
SLX4UTR
(245)
Fit0
Flag-HA-SLX4-SMX

Figure 5

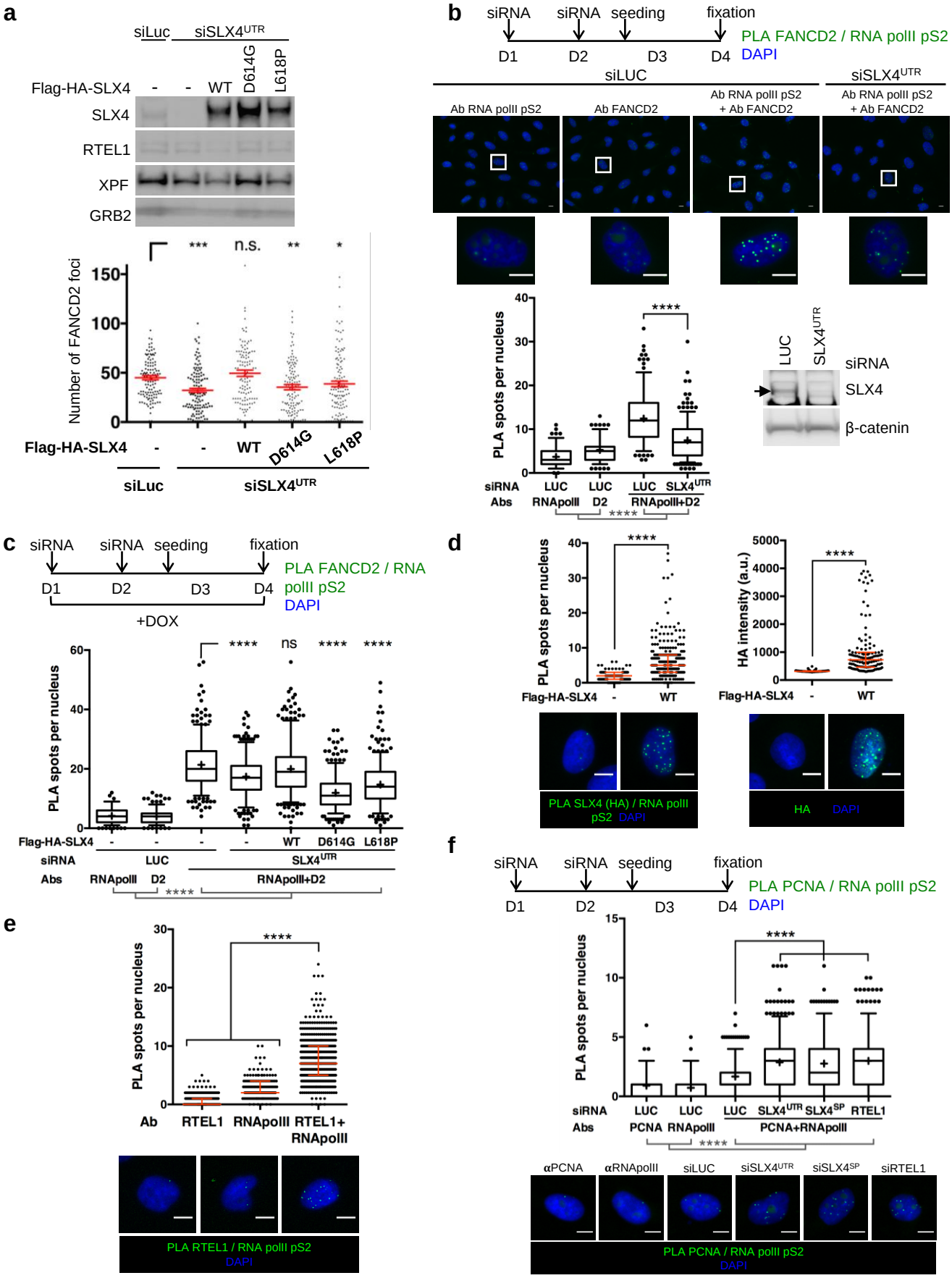
a
siLuc
siSLX4UTR
Flag-HA-SLX4
WT
D614G
L618P
SLX4
RTEL1
XPF
GRB2
Number of FANCD2 foci
n.s.
siLuc
siSLX4UTR
b
siRNA
siRNA
seeding
fixation
D1
D2
D3
D4
PLA FANCD2 / RNA polII pS2
DAPI
siLUC
siSLX4UTR
Ab RNA polII pS2
Ab FANCD2
Ab RNA polII pS2 + Ab FANCD2
PLA spots per nucleus
siRNA
Abs
LUC
SLX4UTR
RNApolII
D2
RNApolII+D2
β-catenin
c
+DOX
ns
d
PLA SLX4 (HA) / RNA polII pS2 DAPI
HA intensity (a.u.)
HA
e
Ab
RTEL1
RNApolII
RTEL1+ RNApolII
PLA RTEL1 / RNA polII pS2 DAPI
f
PLA PCNA / RNA polII pS2
PCNA
PCNA+RNApolII
SLX4SP
αPCNA
αRNApolII
siLUC
siSLX4UTR
siSLX4SP
siRTEL1
PLA PCNA / RNA polII pS2 DAPI

Figure 6

a

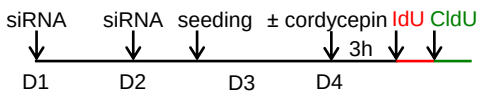
siRNA
siRNA
seeding
± cordycepin
IdU
CldU
3h
D1
D2
D3
D4

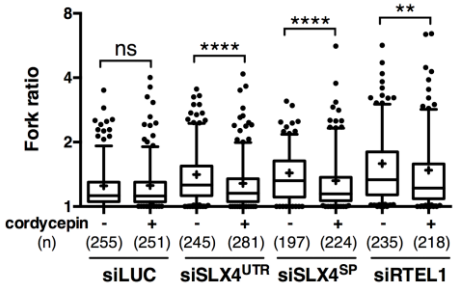
Fork ratio
ns
****
****
**
cordycepin
(n)
(255) (251) (245) (281) (197) (224) (235) (218)
siLUC
siSLX4UTR
siSLX4SP
siRTEL1

b

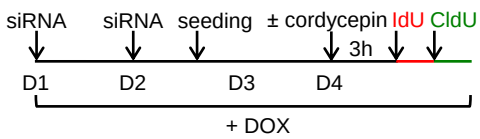
siRNA
siRNA
seeding
± cordycepin
IdU
CldU
3h
D1
D2
D3
D4
+ DOX

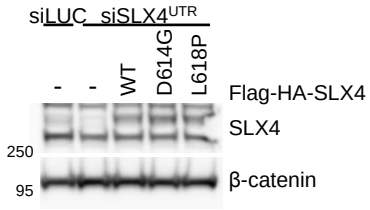
siLUC
siSLX4UTR
-
-
WT
D614G
L618P
Flag-HA-SLX4
SLX4
250
95
β-catenin

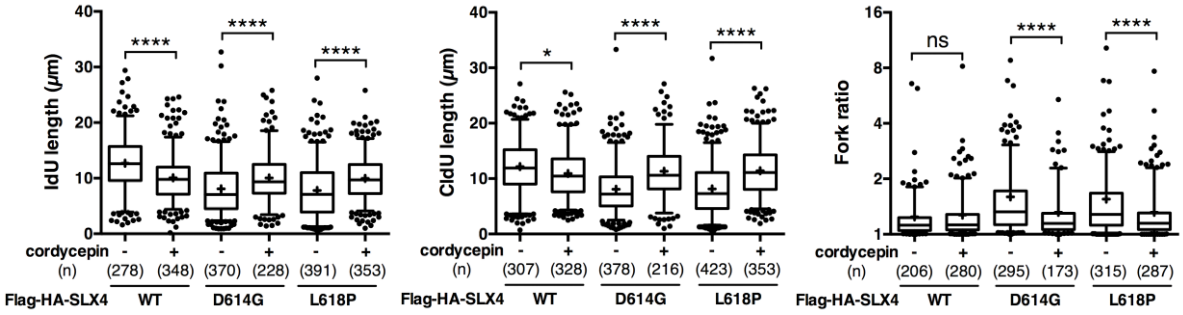
IdU length (μm)
CldU length (μm)
Fork ratio
cordycepin
(n)
(278) (348) (370) (228) (391) (353)
(307) (328) (378) (216) (423) (353)
(206) (280) (295) (173) (315) (287)
Flag-HA-SLX4
WT
D614G
L618P

c

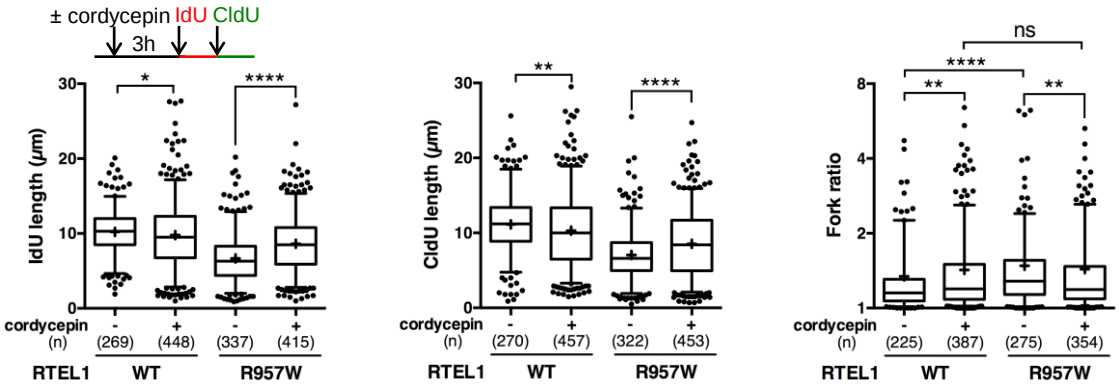
± cordycepin
IdU
CldU
3h
IdU length (μm)
CldU length (μm)
Fork ratio
cordycepin
(n)
(269) (448) (337) (415)
(270) (457) (322) (453)
(225) (387) (275) (354)
RTEL1
WT
R957W

Extended Data Figure 1

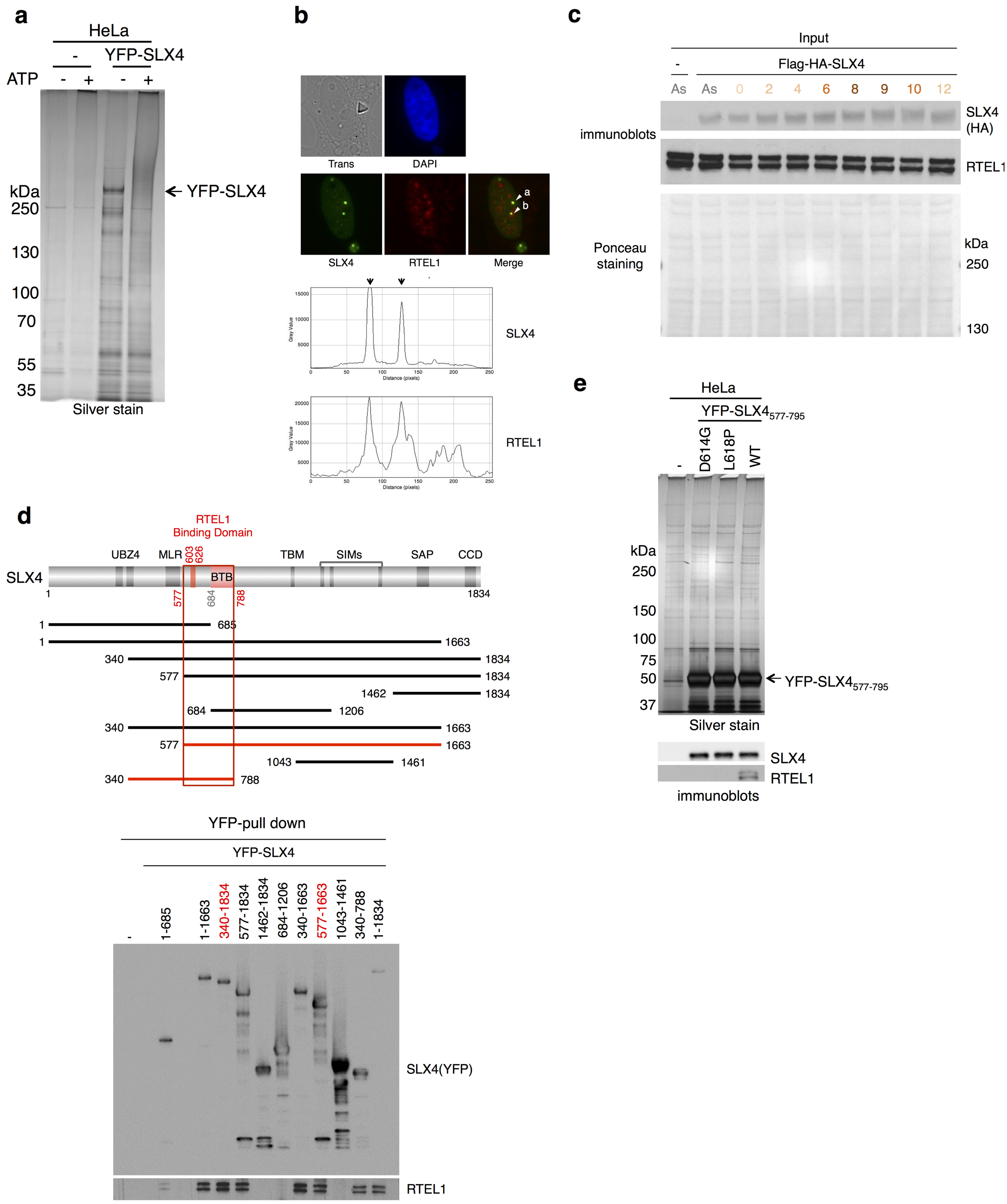

Extended Data Figure 2

		PSM Number (Spectral count)							
		ATP-				ATP+			
		YFP-SLX4 WT		FIT0		YFP-SLX4 WT		FIT0	
		Run1	Run2	Run1	Run2	Run1	Run2	Run1	Run2
Accession	Description	PSM	PSM	PSM	PSM	PSM	PSM	PSM	PSM
Q8IY92	**SLX4**	**423**	**415**			**363**	**353**		
Q9BQ83	SLX1	17	18			18	15		
Q92889	XPF	83	72			71	69		
P07992	ERCC1	28	24			26	23		
Q96NY9	MUS81	20	17			14	15		
P43246	MSH2	31	29			28	25		
Q15554	TRF2	11	8			7	8		
Q96AY2	EME1	17	17			12	11		
Q5VYV7	SLX4IP	9	8			6	5		
Q9NZ71	**RTEL1**	**7**	**6**			**2**	**2**		

Extended Data Figure 3

		PSM Number (Spectral count)											
		YFP-SLX4 WT			**YFP-SLX4 D614G**			**YFP-SLX4 L618P**			**FIT0**		
		Run1	Run2	Run3	Run1	Run2	Run3	Run1	Run2	Run3	Run1	Run2	Run3
Accession	Description	PSM	PSM	PSM	PSM	PSM	PSM	PSM	PSM	PSM	PSM	PSM	PSM
Q8IY92	**SLX4**	**278**	**306**	**311**	**225**	**239**	**243**	**232**	**245**	**247**	**2**	**3**	**2**
Q9NZ71	**RTEL1**	**13**	**12**	**14**									
P81605	Dermcidin	3	4	3									
P12273	Prolactin-inducible protein	3	3	3									

Extended Data Figure 4

a

HD1 extension required for interaction with SLX4 helix

HD1 RTEL1

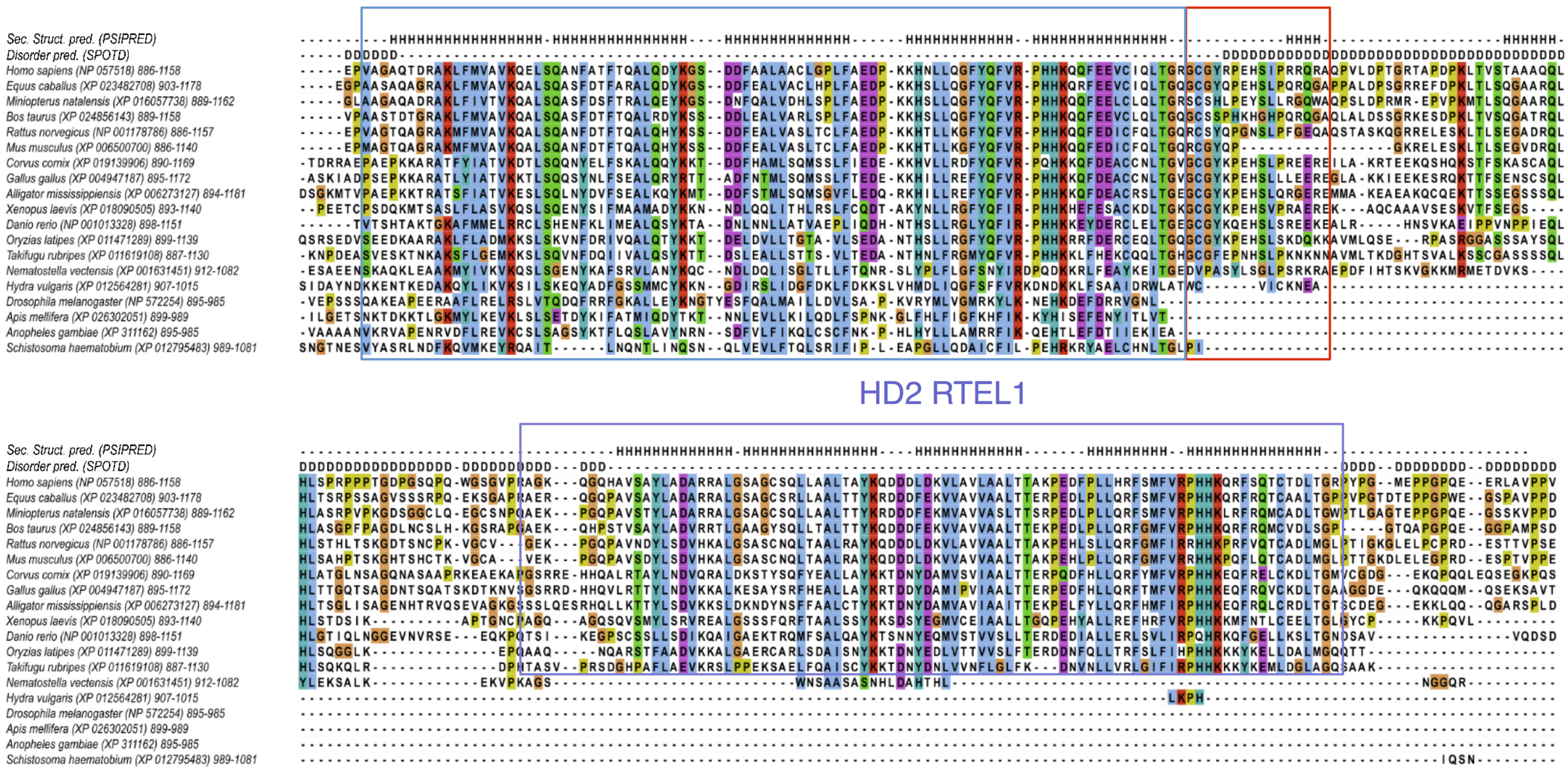

HD2 RTEL1

b

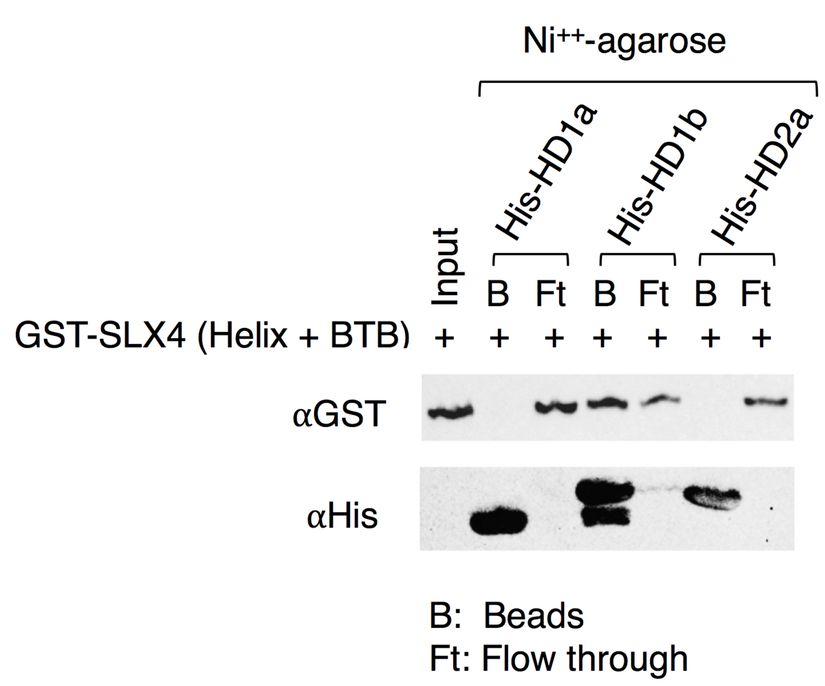

d

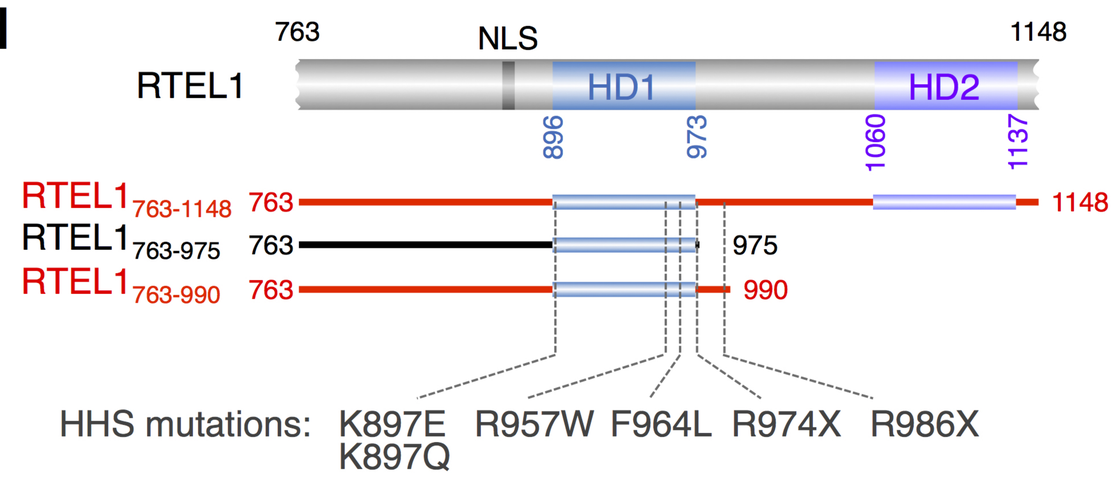

c

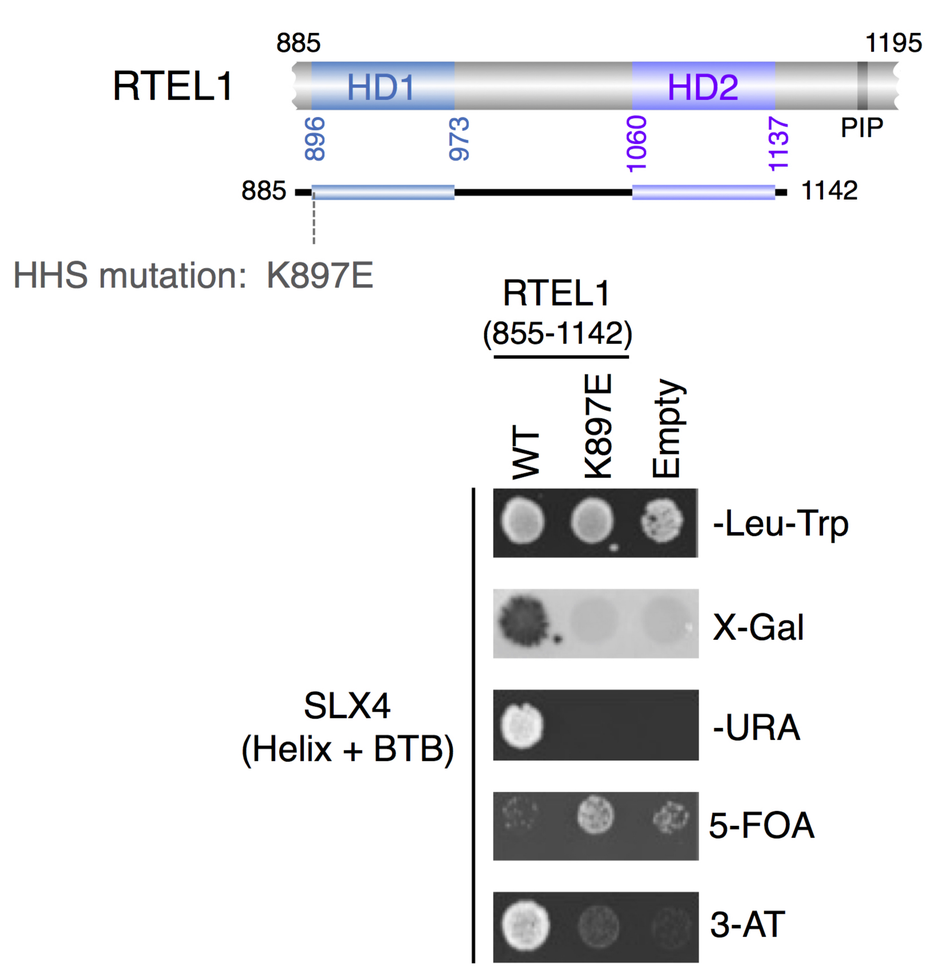

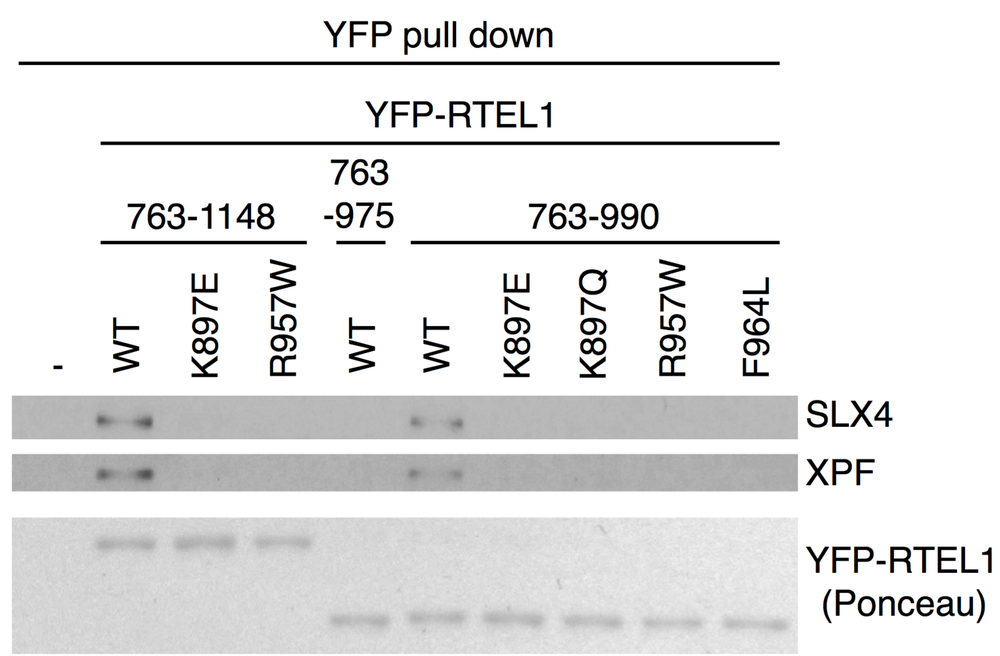

Extended Data Figure 5

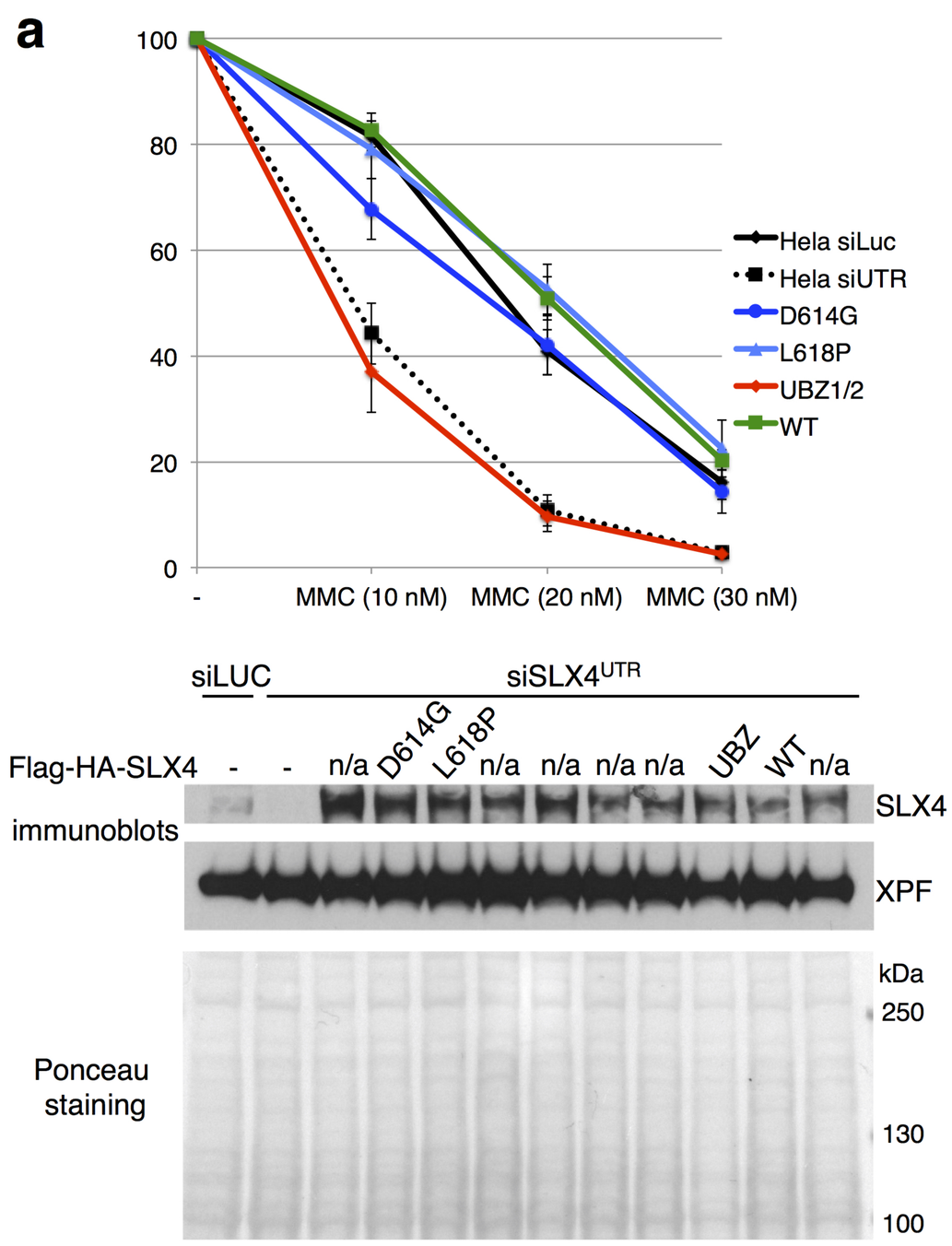

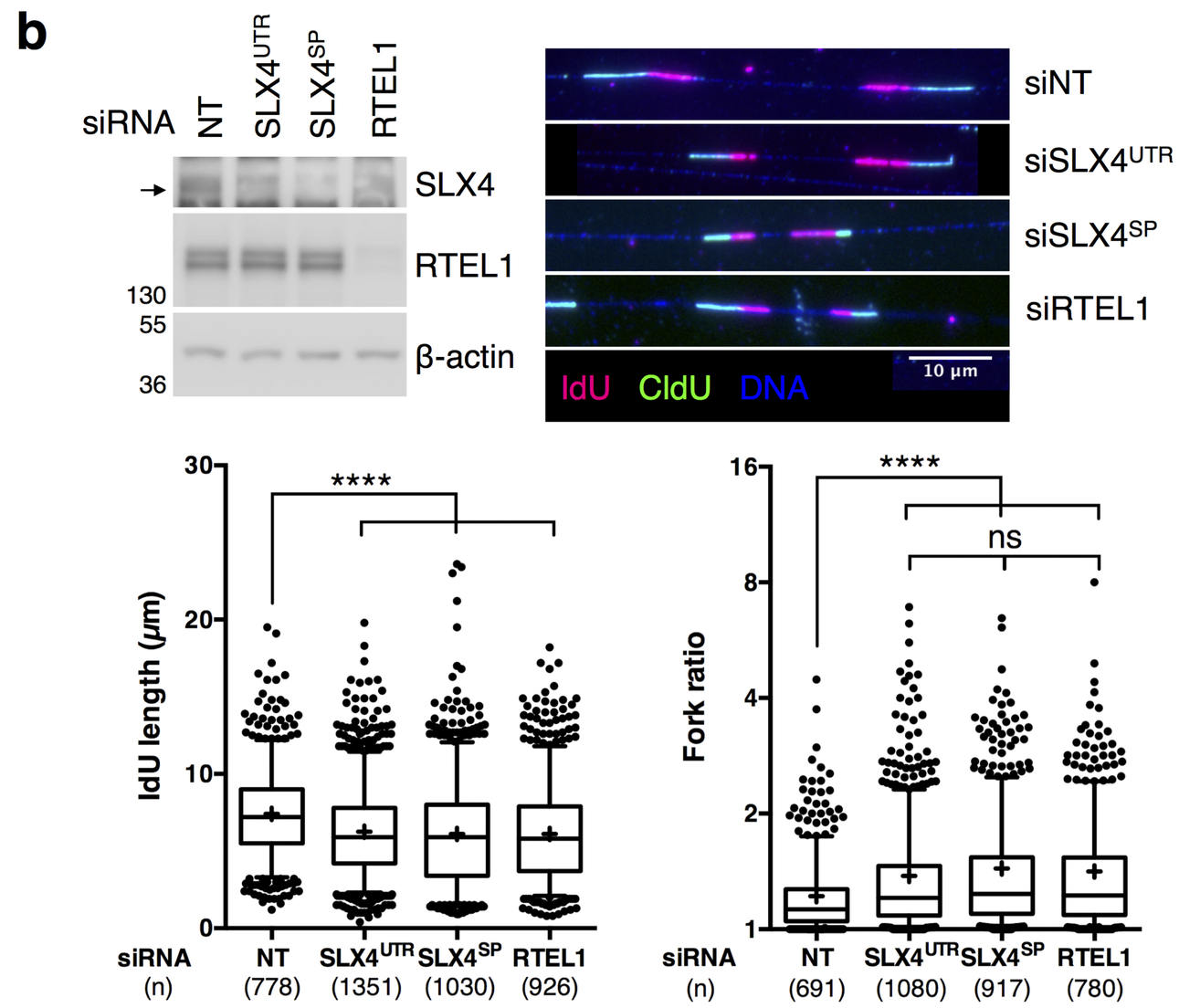

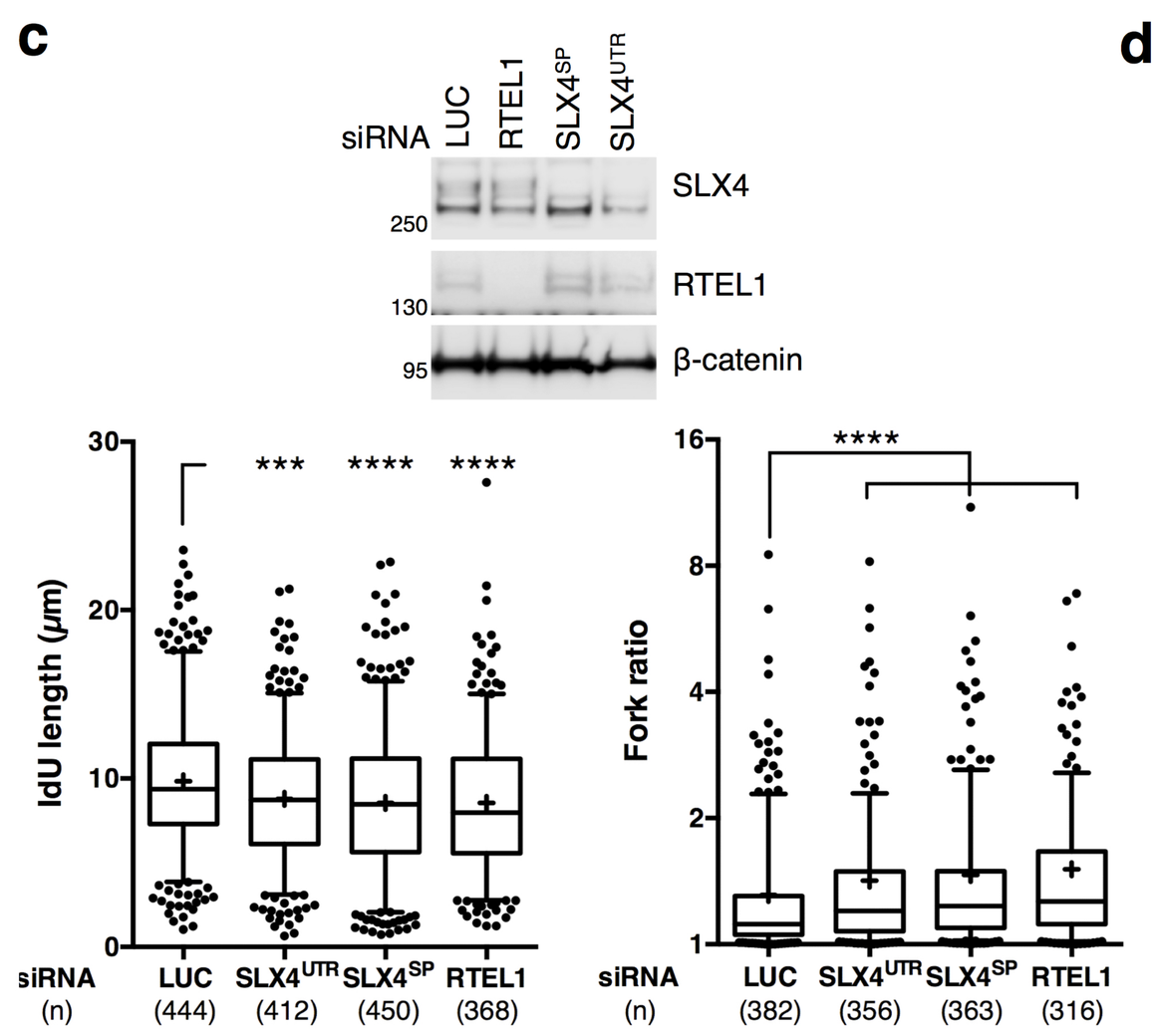

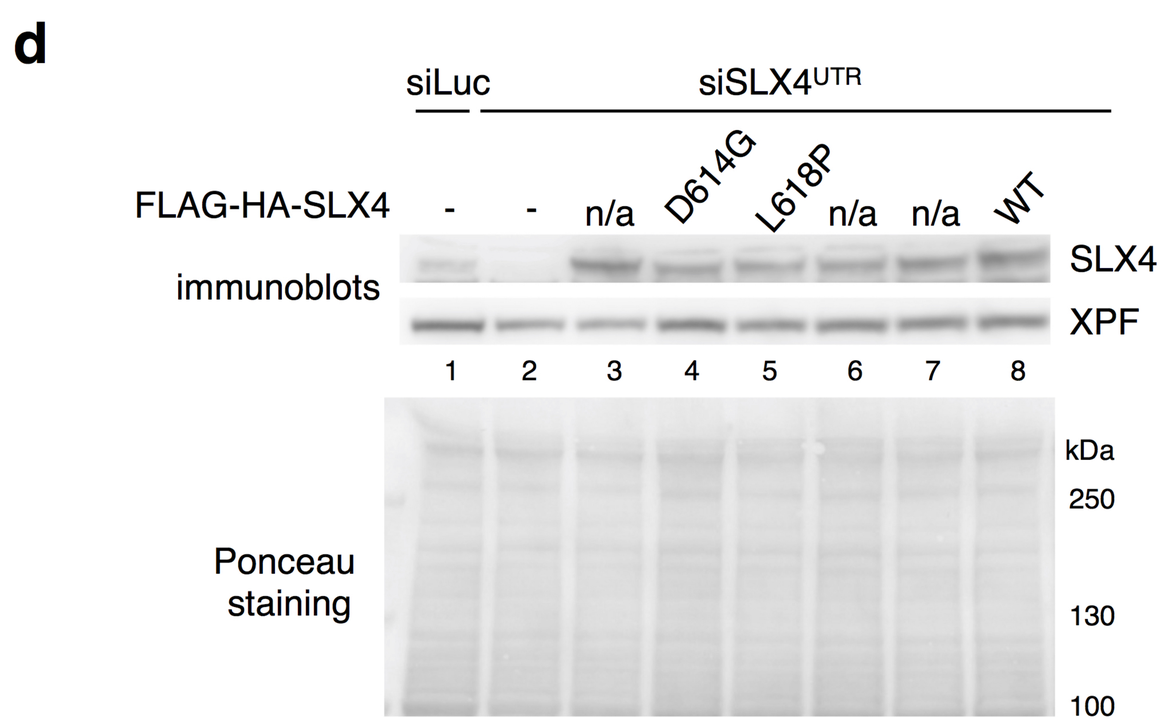

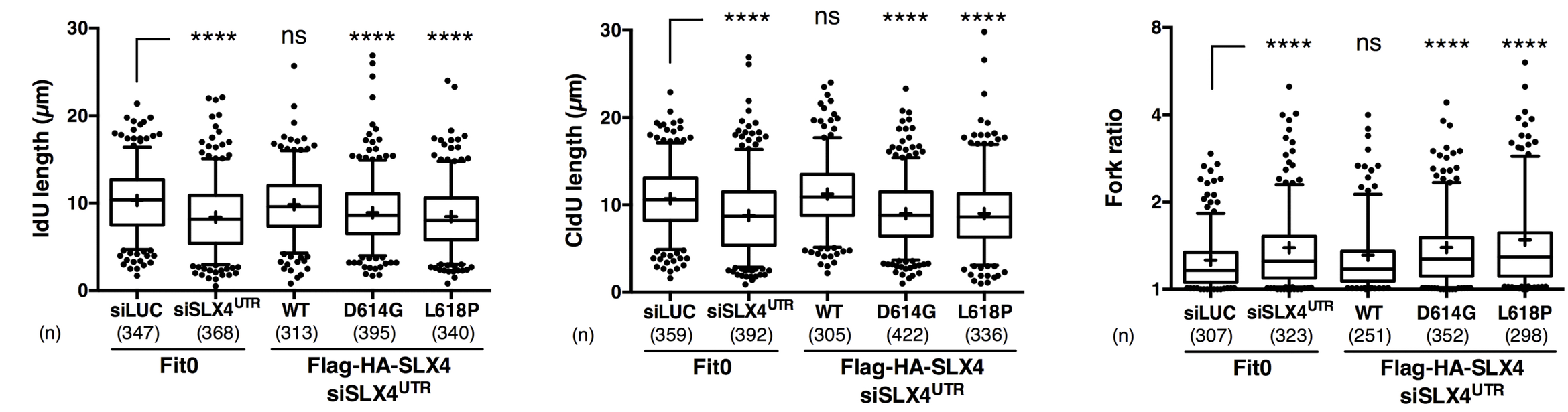

Extended Data Figure 6

a

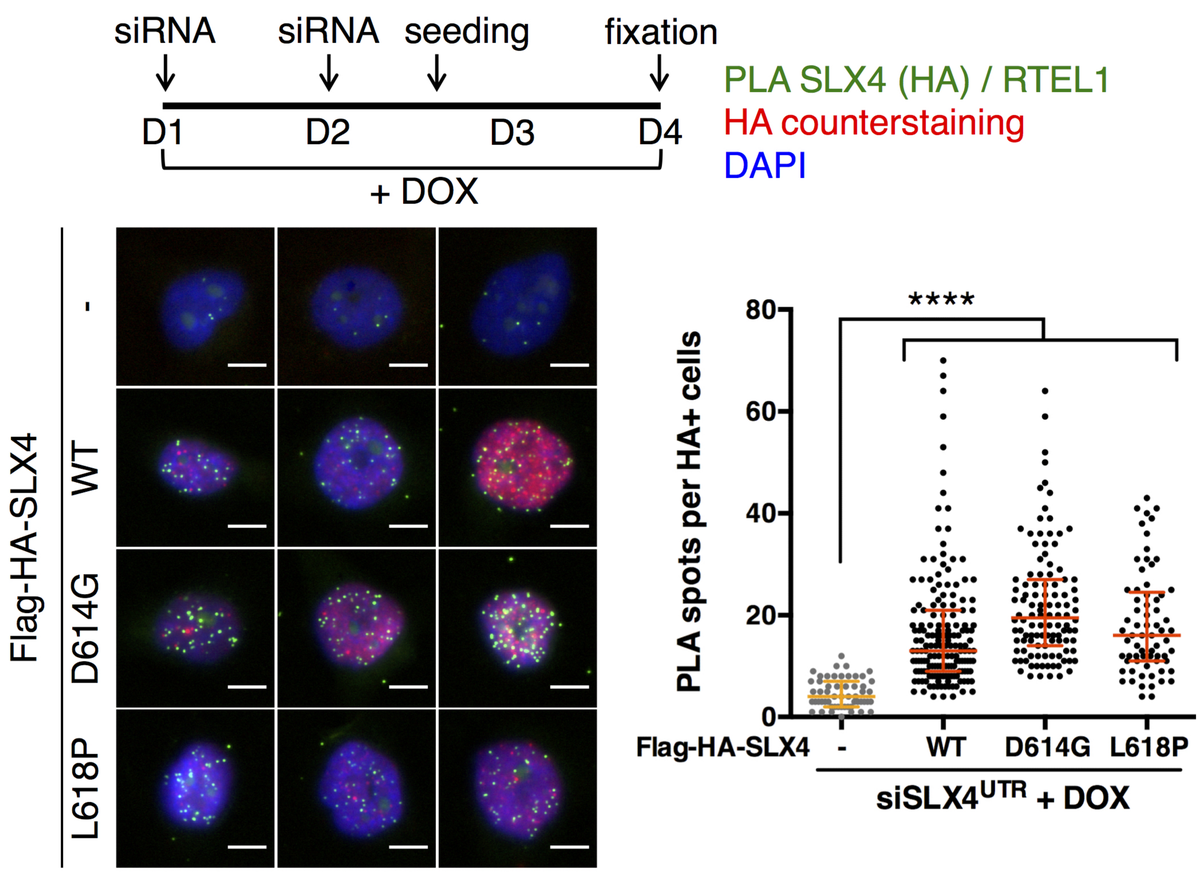

b

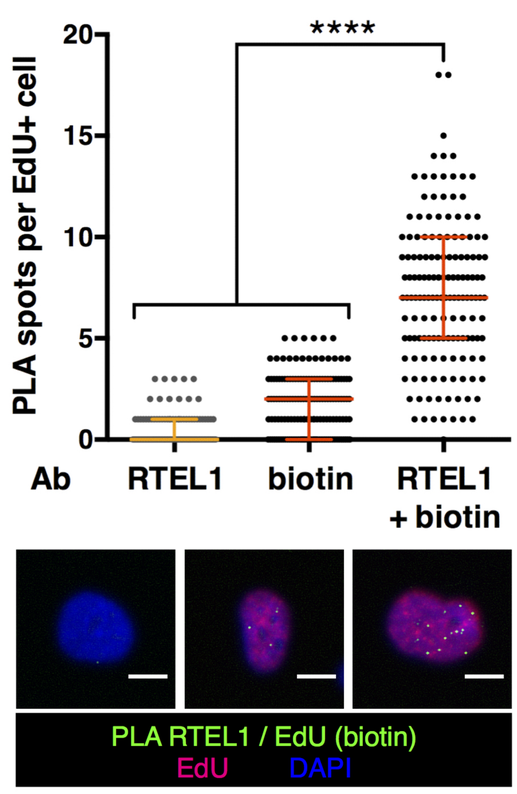
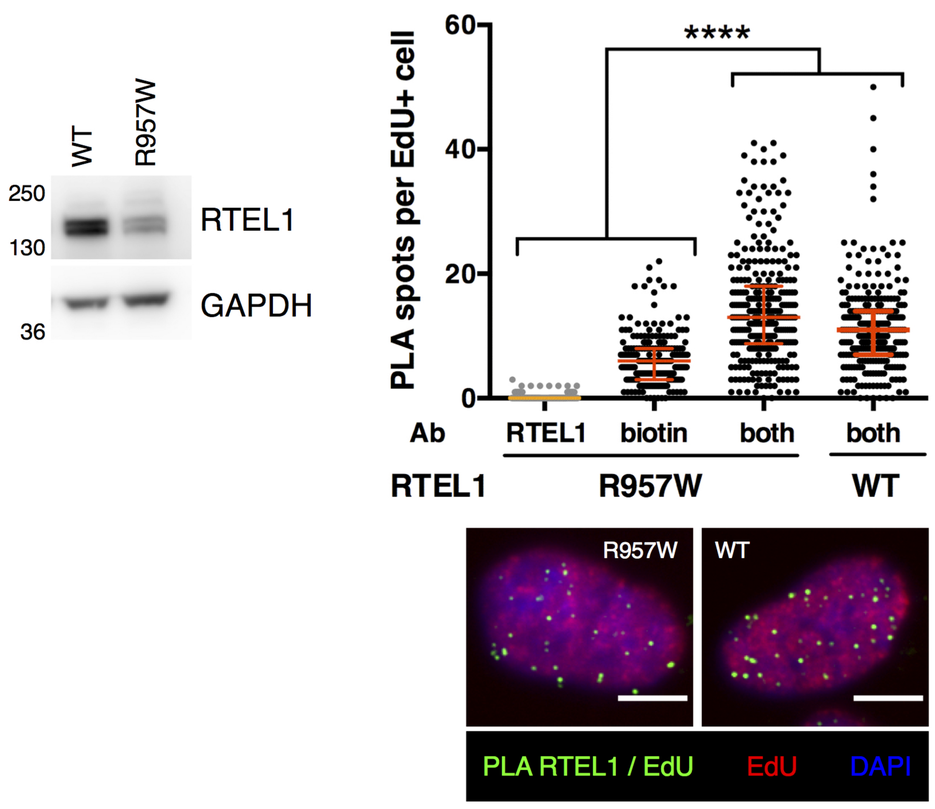
c